DOI:
10.1016/j.actbio.2016.09.040

Document Version
Peer reviewed version

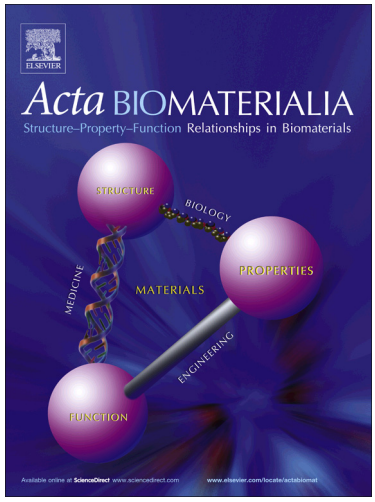

Full length article

Modular peptides from the thermoplastic squid sucker ring teeth form amyloid-like cross-β supramolecular networks

Shu Hui Hiew, Paul A. Guerette, Ondrej J. Zvarec, Margaret Phillips, Feng Zhou, Haibin Su, Konstantin Pervushin, Brendan P. Orner, Ali Miserez

PII: S1742-7061(16)30513-X
DOI: http://dx.doi.org/10.1016/j.actbio.2016.09.040
Reference: ACTBIO 4461

To appear in: *Acta Biomaterialia*

Received Date: 12 May 2016
Revised Date: 23 September 2016
Accepted Date: 28 September 2016

Please cite this article as: Hui Hiew, S., Guerette, P.A., Zvarec, O.J., Phillips, M., Zhou, F., Su, H., Pervushin, K., Orner, B.P., Miserez, A., Modular peptides from the thermoplastic squid sucker ring teeth form amyloid-like cross-β supramolecular networks, *Acta Biomaterialia* (2016), doi: http://dx.doi.org/10.1016/j.actbio.2016.09.040

Modular peptides from the thermoplastic squid sucker ring teeth form amyloid-like cross–β supramolecular networks

Shu Hui Hiew[1,2], Paul A. Guerette[1,2,3], Ondrej J. Zvarec[1,2], Margaret Phillips[4], Feng Zhou[1], Haibin Su[1], Konstantin Pervushin[4], Brendan P. Orner[5], and Ali Miserez [1,2,*]

(1) School of Material Science and Engineering, Nanyang Technological University (NTU), Singapore 639798

(2) Center for Biomimetic Sensor Science (CBSS), NTU, Singapore 637553

(3) Energy Research Institute at Nanyang Technological University (ERI@N), 50 Nanyang Drive, Singapore, 637553

(4) School of Biological Sciences, Nanyang Technological University, Singapore 639798

(5) School of Biomedical Sciences, King's College London, London SE1 1DB

* Author for correspondence: ali.miserez@ntu.edu.sg

Abstract

The hard sucker ring teeth (SRT) from decapodiforme cephalopods, which are located inside the sucker cups lining the arms and tentacles of these squid species, have recently emerged as a unique model structure for biomimetic structural biopolymers. SRT are entirely composed of modular, block co-polymer-like proteins that self-assemble into a large supramolecular network. In order to unveil the molecular principles behind the SRT's self-assembly and robustness, we describe a combinatorial screening assay that maps the molecular-scale interactions between the most abundant modular peptide blocks of suckerin proteins. By selecting prominent interaction hotspots from this assay, we identified four peptides that exhibited the strongest homo-peptidic interactions, and conducted further in-depth biophysical characterizations complemented by molecular dynamic (MD) simulations to investigate the nature of these interactions. Circular Dichroism (CD) revealed conformations that transitioned from semi-extended poly-proline II (PII) towards β-sheet structure. The peptides spontaneously self-assembled into microfibers enriched with cross β-structures, as evidenced by Fourier-Transform Infrared Spectroscopy (FTIR) and Congo red staining. NMR experiments identified the residues involved in the hydrogen-bonded network and demonstrated that these self-assembled β-sheet-based fibers exhibit high protection factors that bear resemblance to amyloids. The high stability of the β-sheet network and an amyloid-like model of fibril assembly were supported by MD simulations. The work sheds light on how Nature has evolved modular sequence design for the self-assembly of mechanically robust functional materials, and expands our biomolecular toolkit to prepare load-bearing biomaterials from protein-based block co-polymers and self-assembled peptides.

Keywords: Self-assembly; Peptide biomaterials; Beta-sheet; Suckerins; Amyloid

1. Introduction

Humboldt (*Dosidicus gigas*) squid have evolved robust sucker ring teeth (SRT) that are embedded within the suction cups coating the inner surfaces of their arms and tentacles. Each appendage contains dozens of SRT,[1] which are formidable biotools that are instrumental to the survival of this ancient predatory creature. SRT represent an intriguing biomaterial exclusively made of proteins called "suckerins" and they exhibit structural properties[2] that match those of robust synthetic polymers, which are based on the supramolecular assembly of suckerins. Inter-chain covalent cross-links are unusually absent in SRT, which are also devoid of the common building blocks observed in load-bearing natural materials such as minerals or chitin.[3] Because of this supramolecular assembly which is stabilized by cooperative weak interactions, SRT exhibit

thermoplastic behavior that make them a functional "bioink" for 3D bioprinting applications.[4] It has also been established that recombinant suckerins are versatile building blocks that can be used to engineer various structural and functional materials, including stable colloids,[5] redox-active substrates for the growth of gold nanoparticles,[6] and as hydrogels whose elastic modulus can be modulated over several orders of magnitude.[7]

We have previously sequenced dozens of genes encoding members of the suckerin protein family.[8] The suckerins are highly repetitive and modular, and assemble into a semi-crystalline supramolecular network consisting of an amorphous matrix reinforced with nano-confined β-sheets.[4, 8, 9] Almost all suckerins consist of peptide motifs that are reminiscent to those found in silk proteins. The first type of module is enriched with Alanine (Ala), Threonine (Thr), and Histidine (His) residues and is predicted to form the β-sheet secondary structure, where the sheet length is precisely constrained by Proline (Pro) residues located on each side of the module, although it is not fully clear yet whether the β-sheets adopt a parallel or an anti-parallel orientation. The second type of module is dominated by Glycine (Gly), with a significant amount of Leucine (Leu) and Tyrosine (Tyr) residues present. These modules are generally longer and are predicted to form the amorphous phase of the network, though the presence of smaller β-sheets in these domains cannot be completely excluded. We hypothesized that the repetitive and modular units greatly contribute to the robust mechanical properties of SRT, and aimed to further understand their behavior in different environmental conditions in order to unveil the physico-chemical factors that are responsible for the material's self-assembly and robustness. We dissected the primary amino acid sequence of the most abundant suckerin protein, suckerin-19 (molecular weight 39kDa, Figure 1A) to identify the key modular units and explore their fundamental interactions at the molecular scale. Importantly, the modular peptides found in suckerin-19 are conserved within most other members of the suckerin gene family,[8] allowing us to investigate peptide sequence designs that are relevant to the entire SRT system.

A combinatorial peptide macroarray interaction assay was first designed to map out the interactions between the modular peptides, which was assessed by fluorescence intensity, whereas dynamic light scattering (DLS) experiments were used to monitor the kinetics of peptide self-assembly. Peptides that showed high relative interactions with this assay were selected for further secondary structure studies by CD and FTIR. Ala-rich peptides were observed to spontaneously self-assemble into micro-fibers and displayed amyloidogenic characteristics, which we suggest may play parallel roles in SRT self-assembly. The stability of these amyloid-like structures was then assessed by hydrogen/deuterium (H/D) exchange, which demonstrated a high protection factor of the residues

involved in the hydrogen bonded network. Finally, MD simulations confirmed the propensity of suckerin-based Ala-rich peptides to form β-sheets, which were highly stable. In contrast, His-rich peptides had low propensity towards β-sheets formation. MD simulations also provided insights into the role of Pro on the stability of the modular β-sheet forming peptides.

2. Experimental Details

2.1. SPOT synthesis

Peptides purchased from GL Biochem were verified with reverse-phase HPLC C-18 and LC-MS to have a high purity of >98% before SPOT synthesis. The protocol for SPOT synthesis was partially modified from Hilpert et al.[10]; coupling cocktail was prepared peptide/HOBt/TBTU/DIEA (1:4.9:4.9:5, eq) in DMF and spotted at 1uL per spot on Whatman Chr1 cellulose, and left to dry before respotting again for 3 cycles to maximize coupling. Thorough washing in DMF with agitation on a lab shaker was done before staining with bromophenol blue in methanol (20-50mg in 1 liter) to check for spots. After destaining of bromophenol blue in methanol, acetylation of the N-terminus α-amino group was done by immersing the cellulose sheet in capping solution of acetic anhydride/DIEA/DMF (1:1:8, vol/vol). Bromophenol blue staining was used to check for the completion of acetylation, and after final destaining with methanol, cellulose sheet was left to dry under ambient conditions.

2.2. Preparation of dye-labeled peptides

Termini-modified peptides (N-terminus acetylated and C-terminus amidated) were labeled at their amidated C-terminus with Texas Red fluorescent dye (Invitrogen, Texas Red SE Mixed Isomers), according to labeling protocol from Invitrogen. Labeling mixture was incubated overnight on vortex and purified with dye removal column (Pierce^{TM}) before diluting with respective blocking buffers (at pH 4, 7 and 8.6) to concentrations of 0.1µM, 0.5µM and 1µM prior to the macro array binding assay.

2.3. Peptide macro array binding assay

Spots were punched out and inserted into a 96-well microtiter plate. Contents of each well were hydrated with methanol for 1 hour then washed 3x with respective buffers (at pH 4 (0.1M Acetate buffer), pH 7 (0.1M Phosphate-buffered saline) and pH 8.6 (0.1M Tris-buffered saline)) prior to incubation with blocking buffers of the same pH with 0.2% Tween 20 and 0.1% BSA for 2 hours on a rocker. Blocking buffer was removed and 40uL of analyte solution containing fluorescently labeled peptides (0.1µM, 0.5µM and 1µM) diluted in blocking buffer was added and incubated for 3 hours on

a rocker. Stringent washings were conducted at the end of the incubation (3x blocking buffer, 3x Tween containing buffer and 3x buffer) before imaging with Typhoon fluorescent imager. All steps were conducted at ambient temperature and in the dark. Each condition was done in quadruplicates to obtain a fair average.

2.4. Dynamic Light scattering

Termini-modified peptides (N-terminus acetylated and C-terminus amidated) were dissolved in buffers of pH 4 (0.1M Acetate buffer), pH 7 (0.1M Phosphate-buffered saline) and pH 8.6 (0.1M Tris-buffered saline), and in urea, at 50μM prior to DLS measurements. All buffers were double filtered prior to use. The Z-average size measurements were collected at intervals of 10 minutes, over a period of 24 hours. Results are presented in 30min segments and error bars are obtained and presented for the data obtained.

2.5. Circular dichroism and FTIR

Termini-modified peptides (N-terminus acetylated and C-terminus amidated) were prepared at 2mg/ml and a quartz cuvette with optical path length of 0.2mm was used. Data acquisition was performed by AVIV 420 Circular Dichroism spectrometer in wavelength steps of 0.5nm at a range from 190-260nm, and with an averaging time of 0.1s over 3 scans. All CD spectra measurements were performed at 25°C. Spectra were plotted using OriginPro9.1 software, averaged over 3 scans and adjacent-averaging smoothing of 10 points was applied for all spectra.

For ATR-FTIR spectroscopy, peptides were prepared at 2mg/ml (0.2%) and spectra were recorded for the peptide in solution with a Bruker Vertex 70 FTIR spectrometer, in the range 400-7500cm^{-1}, with a resolution of 4cm^{-1} and averaged over 280 scans at ambient temperature. Solution samples were homogenized with a vortex mixer prior to being pipetted onto an ATR ZnSe crystal, then spectra were recorded as the samples were dehydrated with steady flow of nitrogen gas. Microfiber samples were obtained by–separating observable self-assembled microfibers from solution. Air-dried microfibers were placed onto the surface of the crystal and pressed down with a sample clamp for spectra measurements. Data processing was performed using OPUS 6.5 software and water compensation and 13-17 point smoothing were applied before calculating the second derivative. Deconvolution of the spectra was done in the spectral range 1600-1700cm^{-1} and peak-fitting was applied with Gaussian band profiles.

2.6. FESEM imaging

All samples were desiccated and coated with Platinum (Pt) at below 5Pa at 20mA for 60 seconds prior to imaging. Samples were imaged at 5.0 kV accelerating voltage, 195 µA emission current and 7µA probe current. Lower secondary electron detector (LEI) mode was used.

2.7. NMR spectroscopy

All NMR spectra were measured at 25^{o}C using 600 (with room temperature probe) or 700 MHz (with cryoprobe) Bruker Avance II spectrometers. NMR data were processed using TopSpin 2.1(www.bruker-biospin.com) and analyzed using CARA (www.nmr.ch). The ^{1}H Chemical shifts were referenced directly to the ^{1}H signal of DMSO peak observed at 2.50 ppm in deuterated DMSO (dimethyl sulfoxide-d6).

Backbone and side chain assignments of all peptides were done using 2D homonuclear NMR experiments such as Total Correlation SpectroscopY (TOCSY) and Rotating frame Overhauser Effect SpectroscopY (ROESY) or Nuclear Overhauser Effect SpectroscopY (NOESY). For 2D TOCSY (containing DIPSI 2 spin-lock sequence) for both peptides A1 and A2, a mixing time of 80 ms was chosen. For peptide A1, 2D ROESY with a mixing time of 200 ms was used while for peptide A2 2D NOESY with a mixing time of 200 ms was used. In both experiments, 256 (t1) and 2048 (t2) points were collected with 16 scans and zero filing was done using 2K X 2K data points along F2, F1 dimensions prior to Fourier transformation.

For H/D exchange studies, the peptides were incubated in their respective buffers for 5 days at a concentration of 2 mg/ml to allow the peptides to self-assemble into microfibers, and subsequently the buffer solution was removed by lyophilization. These microfibers were then exposed to deuterium oxide for a range of 3 days followed by snap freezing and lyophilization. The powder was then dissolved in deuterated DMSO-d_6 and the H/D exchange was followed by 1D ^{1}H NMR experiments. All 1D 1H experiments were recorded with 16K data points and 32 scans with 2 s interscan delay and zero filled to 32K data points.

2.8. Molecular Dynamics Simulation

The simulations were performed by using the GROMACS4.5.3 package.[11-16] The overall temperature of the water and peptides was kept constant, coupling independently each group of

molecules at 300 K with a V-rescale thermostat.[17] The pressure was coupled to a Parrinello-Rahman[17, 18] barostat at 1 atm separately in every dimension. The temperature and pressure time constants of the coupling were 0.1 and 2 ps, respectively. The integration of the equations of motion was performed by using a leap frog algorithm with a time step of 2 fs. Periodic boundary conditions were implemented in all systems. A cutoff of 1 nm was implemented for the Lennard–Jones and the direct space part of the Ewald sum for Coulombic interactions. The Fourierspacepart of the Ewald splitting was computed by using the particle-mesh-Ewald method,[19] with a grid length of 0.16 nm on the side and a cubic spline interpolation. We used the TIP3P water model,[20] and the peptide parameters were from CHARM force field.[21, 22]

2.9. Statistical Analysis

Results of peptide macro array binding assay were analyzed via GelAnalyzer software, and intensities normalized using a control peptide macro array. Each condition was performed in quadruplicate and background (intensities of spots prior to incubation with analyte peptide) subtraction was performed for all spots, with intensities reported in bar charts (Supplementary Information) as mean ± SD (standard deviation) (n = 3-4) with 95% confidence level, where error bars denote SD. Results of NMR H/D exchange studies were performed in triplicate and normalized using methyl peaks. Both NMR H/D exchange studies and Molecular Dynamics simulation are presented as mean ± SD (n = 3), where error bars denote SD. Data acquisition parameters and analysis for CD and FTIR measurements such as number of scans, and deconvolution and smoothing procedures are described in Section 2.5.

3. Results

3.1. Peptide selection

In order to identify the building blocks that drive the self-assembly of SRT structure and that contribute significantly to the robust properties of the material, the fundamental interactions of these building blocks at the molecular level were evaluated. We selected suckerin-19 in this study because ***(i)*** it is the most abundant protein present in the SRT, and ***(ii)*** the modular peptides identified in suckerin-19 are representative of the ensemble of modular peptides present in the entire suckerin protein family that form the SRT supramolecular network.[8] We further refined the selection of peptides based on recent Wide-Angle X-ray Scattering (WAXS) synchrotron experiments of native SRT, which revealed the existence of a network of nano-confined β-sheet structures with dimensions of 2.4-2.6 nm by 3-3.5

nm (estimated 5 strands of ~8-10 residues)[4, 8] that were arranged isotropically within an amorphous matrix. Based on the β-sheet forming propensities of amino acids and the well-known formation of β-sheets in spider dragline silks arising from poly-Ala sequences,[23] we hypothesized that the combination of Ala- and His-rich domains were the likely source of β strands in the nano-confined β-sheet reinforced polymer network. Gly-rich modules, on the other hand, were proposed to form mostly amorphous domains. From these considerations, we identified seven highly abundant and repetitive small peptides (< 8 residues) from suckerin-19 (Table 1), which were classified into three sub-classes of peptides. Type 1 His and Thr-rich modules (**H1**: HTTHHA and **H2**: HTTHHAP); type 2 Ala–rich modules (**A1**: AATAVS and **A2**: PAATAVS), and type 3 modules enriched with Gly, Leu, and Tyr residues (**G1**: GGY, **G2**: GGLY; **G3**: GLGGY). A and H modules in native suckerins are usually flanked by proline (Pro) residues in the form Pro-AH-Pro. Given the established role of Pro as a β-sheet disruptor,[24, 25] we also postulated that Pro restricted the self-assembly of the Ala- and His-rich domains into β-sheets of specific dimensions. Thus **H2** peptide was identical to **H1** with the exception of a Pro residue at the C-terminus. Likewise, **A2** is identical to **A1** with a Pro residue at the N-terminus. It is interesting to note that these His-rich, Ala-rich and Gly-rich peptides possess sequence similarity to various natural protein-based hard biological materials (Table 1).

3.2. Combinatorial peptide macro array assay

A combinatorial peptide macro array interaction assay[10, 26-29] with a suckerin-peptide based library was designed in order to obtain a preliminary screening of peptide interactions and to identify binding interactions of binary peptide combinations (Figure 1B, details of the assay are described in Materials and methods section). All binary combinations of peptides were screened at three different pHs and three analyte concentrations to generate 441 different conditions. For all of our experiments, the selected peptides were also acetylated at the N-terminus and amidated at the C-terminus to eliminate termini charge-charge interactions. pHs were selected (4.0, 7.0 and 8.6) in order to specifically investigate the possible influence of the imidazole ring protonation of His side chains, as well as to mimic the pH environment of the growth and development of the SRT. Indeed, the pH is likely to increase incrementally from the specialized epithelial cells[30-34] which produce the SRT proteins (~ pH 4) to the confined extracellular interface at the base of the SRT, and finally to their final supramolecular self-assembly at the ocean's aquatic pH of about 8.3. The overall goal of the assay was to gain insights into which peptides are the most active in interacting with their counterparts at each pH condition.

The interaction assay, carried out at a concentration of 1 μM analyte incubation, is displayed in the form of a heat map in Figure 1C (detailed bar charts are provided in Figures S1-2). The map enabled the identification of interaction "hotspots" and provided a comparative method to assess the relative strength of peptide-peptide interactions. The main goal of the assay was to identify strong binary homo-interactions to be studied in further details in the present work, but the method also provides information on all other hetero-interactions for future studies. Four main trends were observed. First, for most of the peptides selected, homo- and hetero-peptidic interactions increased in the sequence pH 7.0 > pH 8.6 > pH 4.0, and this trend was particularly obvious for the His-rich peptides. At pH 4.0, where the imidazole ring of His residues is protonated, relatively weak interactions were observed, a trend that was observed in the case where the peptide was the ligand (immobilized on the membrane) and where the peptide was the analyte (free flowing solution over the immobilized ligand), as well as for both homo- and hetero-interactions. Moderate interactions were observed at pH 8.6 (deprotonated His residues), whereas the highest interaction activity was obtained at pH 7.0, corresponding to partial protonation of His residues. The protonation state of His thus appears to be an important factor in mediating peptide-peptide interactions. Second, Ala-rich and His-rich peptides generally exhibited the highest interaction activities. Gly-rich peptides, on the other hand, generally exhibited low activity at the varying pHs, especially for the homo-peptidic interactions, suggesting that these sequences are not actively involved in strong binding interactions within the protein, although it should be mentioned that moderate hetero-interactions of **G3** peptide with **H1** as the analyte were observed at pH 7.0 and 8.6. The weak-to-moderate interactions of Gly-rich peptides is consistent with the suggestion that Gly-rich sequences mostly constitute the amorphous regions of the semi-crystalline SRT polymer network, which is similar to sequence/structure relationships observed in silk.[23, 35] However, **G3** peptide displayed a moderate interaction activity, suggesting that it may also be involved in non-amorphous interactions, a possibility that is currently under investigation and will appear in a follow-up publication. Third, the ligand-analyte roles are not identical, with an asymmetric pattern observed across the diagonals of the heat map. Short peptides (< 8 residues long) selected for this study were likely to have been conformationally restricted when immobilized on one end, while the analyte peptides are not limited by such conformational restrictions. This conformation-restriction effect may be more pronounced for shorter peptides, therefore an asymmetric pattern across the diagonals was not unexpected. As the purpose of this screening assay was to identify interaction hotspots when the peptides play both roles as ligand and analyte, the assay provides a broader perspective of the interaction possibilities and the asymmetric pattern did not affect our objectives of

using this macro screening assay to gain a broad picture of the nature of suckerin peptide interactions. Peptides with hotspots in the interaction map were then examined in greater detail.

3.3. Self-assembly of peptides

Based on our combinatorial assay results, peptides exhibiting the highest homo-peptidic interaction activities, **A1** and **H1**, were selected for further analysis. Peptides **A2** and **H2** were also investigated to examine the effect of flanking Pro residues as explained above. During peptide incubation at 2 mg/ml, prominent differences were observed between Ala-rich and His-rich peptides. Ala-rich peptides spontaneously formed aggregates and subsequent Scanning Electron Microscope (SEM) observations indicated that these aggregates consisted of microfibers made up of smaller nanofibrils (Figure ~~5~~2A-F). The fibrils appeared to be of uniform dimensions of *ca.* 30-50 nm thick with some evidence of bundling to form microfibers larger than 1 µm in diameter. The microfibers were stable when subjected to sonication and to a strong denaturing solution of 8M urea. In stark contrast, His-rich peptides **H1** and **H2** did not form any noticeable microfibers under any of the conditions tested. To further assess the assembly of the microfibers, we assessed their kinetics of formation using Dynamic Light Scattering (DLS) measurements at 50 µM peptide concentration and under identical pH conditions used in our macroarray and peptide incubation assays (Figure 3). For all DLS measurements, it is important to note that the polydispersity (PDI) index was expected to be large due to the broad distribution of the peptide oligomeric populations present during self-assembly. Therefore, we view the absolute size values as estimations, with the main objective of monitoring the general trends of peptide oligomerization over time. At pH 7, the *z*-average size, or cumulant mean size of **A1** and **A2** peptides increased as soon as the peptide incubation was initiated (Figure 3C-D). At pHs 4 and 8.6, on the other hand, only minimal changes in peptide sizes were observed by DLS, which is consistent with the weaker interaction activity measured in the macroarray assay. For peptide **A2** (pH 7) the z-average size of the peptides reached a maximum value of *ca.* 15 µm, followed by an apparent decrease in size (Figure 3D). This peak value coincided with the formation of microfibers which sedimented as they formed and which did not contribute to light scattering. We thus attribute the apparent size decrease to the presence of the remaining soluble peptides that did not contribute to the assembly of larger, sedimented microfibers during measurement. The presence of Pro at the N-terminus (peptide **A2**) lead to some noticeable growth at pH 8.6, with z-average size values in the range 1 to 2.5 µm, whereas no growth was observed for peptide **A1** (Figure 3C).

His-rich peptides displayed a similar trend to Ala-rich peptides, namely the oligomer size of **H1** only increased at pH 7 (although this size was significantly smaller than those observed for **A1** and **A2** peptides), whereas no growth was measured at either pH 4 or 8.6 (Figure 3A). The effect of Pro at the C-terminus (peptide **H2**) parallels the findings of Ala-rich peptides (Figure 3B), namely oligomeric assembly was noticed at pH 8.6, which was clearly distinct from the behaviour of peptide **H1** where no size increase was detected. In summary, DLS measurements indicated that: *(i)* peptide aggregation/fibrillization is highly dependent on pH and is maximum at pH 7; and *(ii)* terminally positioned Pro residues affected oligomerization only at pH 8.6.

3.4. Circular Dichroism studies

In order to investigate whether suckerin peptides exhibited significant secondary structural changes[36] in solution over time, Circular Dichroism (CD) studies were conducted at 2 mg/ml peptide concentration under the same pH conditions to those described above and over a time period of up to 50 days. The pH strongly affected conformational transitions over time and such transitions were particularly obvious at pH 7. For His-rich peptides at pH 4, the spectra did not significantly change over time and consisted of intense minima at 195-200 nm and of weak positive broad shoulders near 220 nm, see for instance Figure 4 row 1 for **H1** peptide. Systematic investigations by CD of β-sheet-rich proteins[37] have demonstrated that this spectral signature can be assigned to so-called β_{II}-type proteins, which are β-sheet-rich proteins that also contain short stretches of poly(Pro)II-like conformations (PPII).[38] According to Sreerama and Woody,[37] β-sheet proteins can be classified as β_I or β_{II}, respectively, with the main difference arising from their PPII to β-sheet ratio. This ratio is less than 0.4 in β_I proteins and larger than 0.4 in β_{II} proteins. In turn, the CD signature of β_I proteins exhibit the typical maxima and minima near 195 and 210-220 nm, whereas that of β_{II} proteins have a intense minima at 195-200 nm and a weaker maxima at *ca*. 220 nm.[39] These features are consistent with **H1** peptides at pH 4. Over time, the CD spectra did not change significantly, although the molar ellipticity increased at 7 days and then remained unchanged until 50 days. Very similar CD spectra were observed at pH 8.6 for **H1** peptide (Figure 4 row 3), where the spectra can essentially be separated into two sub-groups, namely 0 and 7 days and at 14 and 50 days. While the minima and maxima are located around the same wavelength, the molar ellipticity decreased for the 14 days and above experimental sets.

For **H1** peptide at pH 7, much more dramatic changes in CD spectra were observed (Figure 4 row 2). The initial spectrum at day 0 was again characteristic of β_{II} proteins. However, the molar ellipticity

sharply decayed over time. After 7 days, the minimum at 195 nm was about 3-fold lower than its initial values. At days 14 and 50, the molar ellipticities were just a fraction of their initial values, and a zoom-in view in the low intensity region (Figure 4 row 2, insets) revealed spectra characteristic of the standard β_I type proteins, with the typical maxima at 195 nm and a broad negative minima centered at 220 nm. Given the propensity of His-rich peptides to form larger oligomeric populations over time as observed from DLS measurements (Figure 3A-B), the large decay in ellipticity values suggested that the peptide concentration in solution drastically decreased as peptides aggregated into larger oligomeric states and sedimented. Furthermore, the residual soluble peptides trended towards β_I-type protein conformation. In this case, the role of Pro appeared to be marginal, with similar overall spectral features for **H2** (Figure 4 for **H2** peptide) compared to **H1** peptide. The one notable difference was that in comparison to **H1** peptide, the CD spectra of **H2** peptide at pH 4 and 8.6 did not change over time, with the intensity at day 50 remaining essentially the same as at day 0. At pH 7, a comparable large decrease in intensity was observed over time, and the residual peptides in solution also exhibited β_I-type structure (Figure 4 row 2, inset).

Ala-rich peptides exhibited slightly different CD spectral features (Figure 4 for **A1** and **A2** peptides), but the same general trends were observed with respect to the role of time and pH. For peptide **A1** (Figure 4 for **A1** peptide) at pH 4, the most prominent characteristics were intense minima at 195-200 nm and secondary negative shoulders at ~ 220 nm. These features were also characteristic of β_{II}-type polypeptide,[37] and have also been reported for short peptides shown to adopt the PPII conformations.[40-42] The location of these characteristic features and the ellipticity values did not evolve significantly over time. At pH 8.6, the CD spectrum of **A1** was initially similar at day 0 and day 7. However, over time the molar ellipticity decreased, and at 50 days the main minima shifted slightly towards lower wavelengths. At pH 7, similar to His-rich peptides, spectral changes were much more distinct, with the ellipticity values strongly decreasing by several orders of magnitude (Figure 4 row 2). Based on DLS and microscopy observations, our Ala-rich peptides rapidly self-assembled into fibrillar structures. Thus the dramatic decrease in intensity is likely related to depletion of peptides from the solution. Closer inspection of the low-intensity region (Figure 4 row 2, inset) indicated that the residual peptides in solution were in the β_I-protein conformation, which could reflect an increased proportion of peptides forming β-sheets. Given the very small intensity values, we however view the spectral changes at day 28 and above with a level of circumspection. Finally, the presence of Pro at the N-terminus (**A2** peptide) did not dramatically affect the CD spectra (Figure 4 for **A2** peptide). The main differences with **A2** were a regular decrease in ellipticity values at pH 4 (while it remained

constant with **A1**) and a lack of shift for the 195 nm minima. At pH 7, the large ellipticity decrease observed over time for **A1** was again clearly apparent for **A2**.

3.5. Complementary ATR-FTIR studies

In order to complement the conformational information obtained by CD, we also investigated the peptides by Attenuated Total Reflection Fourier Transform Infrared Spectroscopy (ATR-FTIR). Two main characteristics of the peptides were of specific interest. First, we wanted to confirm the main structural features of the peptides in solution as measured by CD. Second, we were interested in characterizing the self-assembled microfibers, *i.e.* in the solid state, data that was not accessible with our CD equipment. For the characterization of peptides in solution, we specifically focused our attention to the peptides at pH 4 since both DLS and CD experiments indicated that the peptides exhibited minimal conformational changes and self-assembly at this condition, which thus represented the most stable state in solution. For self-assembled fibers, the combination of DLS and CD indicated a rapid fibrillization of peptides in solution at neutral pH. This was especially prominent for Ala-rich peptides where visible fibers could be seen with the naked eye at all three pH values tested. Hence, in this case ATR-FTIR measurements were conducted on self-assembled **A1** and **A2** microfibers that were separated from the solution.

FTIR spectra of peptide solutions incubated at pH 4 and after 50 days are shown in Figure S4. Semi-quantitative analysis was obtained by deconvoluting the Amide I band using the OPUS 6.5 software, with peak positions[43, 44] for the different secondary structures assigned from the maxima of inverted second derivative of the spectra. For all peptides, the Amide I band was centered at 1620-1622 cm^{-1} indicating β-sheet enrichment. Peak integration of the deconvoluted Amide I band was used to estimate the secondary structure contributions. All four peptides exhibited high β-sheet content in excess of 60 %. Since water is well-known to affect the Amide I band and can thus lead to artifacts with respect to relative secondary structure content estimates, all samples were also measured in their dehydrated state, which was obtained by steadily blowing nitrogen gas over the adsorbed peptide solution. In this case, no significant differences were observed for the His-rich peptides **H1** and **H2** (Figure S4). For Ala-rich peptides, on the other hand, there was a noticeable increase in β-sheet content with above 80% β-sheet content estimated for the dehydrated peptide solution (Table T1), which may not only reflect that Ala-rich peptides have a very high β-sheet content, but also a β-sheet enrichment upon desolvation, a common mechanism in Amyloid fibers.[45] While quantification of protein secondary structure by ATR-FTIR must be judged with caution, including for amyloid-like

peptides[46] this semi-quantitative analysis nonetheless allows us to conclude that all peptides exhibit a high propensity for β-sheet formation, thereby supporting our CD data.

ATR-FTIR analyses of solid state microfibers formed by Ala-rich peptides are shown in Figure 5. The most prominent contribution of the Amide I band was unambiguously located at 1621 cm^{-1} and semi-quantitative analysis of all peptides confirmed a β-sheet content of *ca*. 70 % for both **A1** and **A2** peptides. As a final confirmation that the aggregated microfibers were enriched with β-sheets, they were also stained with Congo red and analyzed under polarized light microscopy.[47, 48] In this case, the microfibers displayed the characteristic apple green birefringence of Congo-red positive structures (Figure 2A-F) characteristic of cross-β structures.[49] Positive controls of the amyloid peptide GGVVIA[50, 51] confirmed the same birefringence characteristics (Figure S3). Taken together, ATR-FTIR and the Congo red staining assay allow us to conclude that Ala-rich peptides assemble into cross-β structures, the characteristic feature of amyloidogenic peptides.

3.6. 1D ^{1}H H/D exchange NMR

The rapid self-assembly of Ala-rich peptides into fibrillary structures, together with CD and FTIR measurements as well as Congo red staining, all point toward a β-sheet-rich fibrillization process which is reminiscent to amyloid formation.[52] In order to gain a deeper understanding of the stability of residues involved in stabilizing these β-sheet rich fibrils, we subjected the microfibers to hydrogen-deuterium (H/D) exchange and NMR spectroscopy, according to a method previously developed to identify residues constituting the amyloid core.[53] In brief, the method identifies the core residues involved in hydrogen bonding by monitoring which backbone amides of the β-sheet stabilized fibrils are the most susceptible to H-bonding disruption. Accordingly, when the fibrils are exposed to deuterium, the labile backbone amide protons exchange with deuterium at a rate controlled by the extent of solvent exposure. DMSO-d_6 was used to dissolve the peptides after D_2O exposure as it slowed down the H/D exchange as opposed to aqueous buffers[54] and breaks down the microfibers into their monomer units.[55] Full details on the exchange procedure are provided in the Supplementary Information.

Chemical shift assignments (Figures S5-8) for the two peptides **A1** and **A2** in DMSO-d_6 were first obtained using 2D TOCSY, ROESY and NOESY spectra,[56] as illustrated in Figures S5-8. Each spin system within the residue as well as the sequential assignment of **A1** could be readily identified. However, for **A2** we observed two sets of peaks for the last two residues (Val6 and Ser7) that were

undistinguishable due to severe overlap. We suggest that these pairs of peaks in the **A2** peptide arise due to cis-trans isomerization of Pro1, resulting in the presence of multiple conformations in solution that manifests as multiple peaks in the 1D 1H NMR spectra (Figure S10). Peptide microfibers dissolved in DMSO-d_6 were used for the reference spectrum and the degree of exchange for each residue was calculated as the peak intensity ratio (signal-to-noise ratio, S/N) of the residues for the exposed and the reference samples, respectively. A characteristic series of 1D ^{1}H spectra for peptide **A1** and **A2** at various H/D exchange incubation temperatures is shown in Figure 6A and C. The corresponding S/N ratio calculated from the 1D series are plotted as a function of temperature in Figure 6B and D for both **A1** and **A2** peptides. All residues of **A1** (Figure 6B) displayed high signal intensity even after three days of exposure to D_2O at temperatures of up to 85°C, indicating that the residues are uniformly and highly protected from the solvent and that they are involved in a tight network of H-bonded β-strands throughout the microfibers. The exchange rates and protection factors of the fibers are comparable to those of robust Aβ(1-42) and Aβ(25-35) amyloid fibrils.[53, 57]

While the H/D exchange for all residues generally increased with temperature, we note an abnormal behaviour at 45ºC, where all residues not only exhibited a higher exchange than at 65ºC but also a large fluctuation in peak intensity, which is evidenced by the large error bars. It is important to note that such high standard deviations appear to be especially prominent at 45ºC and not at other temperatures, indicating that it represents an intrinsic feature of the peptide but is not due to experimental uncertainties. We suggest that **A1** peptide exhibits a phase-transition near this temperature, thereby inducing conformational changes that result in large variability in H/D exchange. Temperature-induced phase transition of peptides is not an uncommon phenomenon[58] and has been documented in amyloid β-peptides as well.[59] These observations will be investigated in greater detail in subsequent studies. We also observed the S/N intensity ratios of residues in **A2** peptide were lower than their counterparts from **A1** peptide up to 65ºC (Figure 6D), indicating that the N-terminal Pro present in **A2** leads to a slightly higher solvent accessibility and that the packing of the β-sheet network is perhaps more relaxed in this case.

3.7. Molecular dynamics simulations

Based on the experimental evidence that suckerin peptides self-assemble into β-sheet rich fibrillar structures with a high structural stability, and with our previous understanding that native SRT are semi-crystalline biopolymers in which nanoconfined β-sheets[8] represents the crystalline phase, a plausible structure for the SRT peptides investigated in this study can be proposed. Accordingly, the

peptides are stacked into anti-parallel β-strands, with the strands oriented perpendicular to the fibrils axis and hydrogen bonds parallel to the fibril axis, namely the classical cross-β structure observed in amyloid fibrils.[46, 52] In order to verify whether our peptides could form stable cross-β supramolecular lattices which would explain the meso- and macroscopic assembly of the fibrils and microfibers we observe, we performed molecular dynamic (MD) simulations of all four peptides using the GROMACS4.5.3 package.[11-16] Specifically, the peptides were arranged into oligomeric lattices made of three extended chains, thereby imposing an initial conformational bias towards anti-parallel β-strands similar to the work reported by Rauscher *et al* on elastin and amyloid fibers.[25] Simulations were conducted in explicit water and allowed to relax in an unconstrained fashion, and the evolution of the lattice was monitored for up to 200 ns (Table T2). In addition to assessing the stability of the oligomeric cross-β networks, the aim of these simulations was to gain further insights into the role of pH and flanking Pro residues. The suckerin peptide based cross-β lattices were assessed under aqueous conditions at different pHs (pH 4.0 and 7.0).

Whereas the **H1** peptide lattice evolved towards a disordered structure at both pH 4.0 and 7.0 (Figure 7C), **H2** peptide exhibited a distinct behaviour, with low-range order partially maintained at pH 7 (Figure 7D). To quantify the relative stability of β-sheets, we compared the H-bond and β-sheet counts at 0 and 200 ns. At both pHs, a higher number of H-bonds were recorded for the lattice made of peptide **H2** in comparison to the lattice made of **H1** after 200 ns simulation (Figure 7A). More obvious distinctions between the peptides were obtained in terms of β-sheet content, with no β-sheet predicted for **H1** (β-sheet count = 0) and a significant amount of β-sheet for **H2** (β-sheet count = 19), which was notably higher at pH 7 (Figure 7B). These results are consistent with the destabilization of the lattice at pH 4 due to the protonation of the imidazole ring, resulting in electrostatic repulsion of adjacent peptides. They also indicated that the C-terminal Pro in peptide **H2** stabilized the β-sheet network, with no clear influence of His residue protonation state. Lattices constructed from Ala-rich peptides displayed a much higher propensity towards β-sheet stabilization of the lattices, which were highly stable under both acidic and neutral conditions (Figure 7E and F). The stability of the β-sheet network was particularly apparent from the β-sheet counts, which were well in excess of those computed for His-rich peptides, with a β-sheet count close to 200 (Figure 7B). We note that at time 0, a higher β-sheet content was obtained for **A1** peptide compared to **A2** peptide. However, after 200 ns the β-sheet content in **A1** decreased, whereas that of **A2** increased, resulting in a higher β-sheet content for the Pro-containing **A2** peptide. The stability of Ala-rich peptides was not affected by pH, which is not

surprising given the absence of titratable side-chains in these peptides. We emphasize that the cross-β lattices that were constructed in these simulations only represent approximations of the actual β-structures of the SRT peptides, which will need to be refined once structural data become available (for instance by x-ray crystallography or solid-state NMR). Notwithstanding these limitations, we can make general conclusions from the *MD simulations*, namely that Ala-rich peptides are able to form highly stable amyloid-like cross-β lattices under most conditions. His-rich peptides, on the other hand, display a much lower β-sheet forming potential, which is nevertheless favorable under conditions when the imidazole ring is deprotonated.

4. Discussion

SRT are entirely constructed from a family of modular, block co-polymer-like proteins. Because of their extreme repetitive primary amino acid sequences, a reductionist approach focusing on the interactions between the most abundant peptide building blocks was undertaken in this study. Three major types of modules were initially selected, namely Gly-rich, Ala-rich, and His-rich modules. It is notable that these modules share sequence similarities with other peptides present in protein-based biological materials. Ala-rich motifs resemble β-sheet forming regions of spider dragline spidroins [60-63] and Gly-containing motifs are highly similar to the sequences constituting the amorphous regions of these silk proteins.[60] Both Ala and Gly-rich motifs also exhibit resemblance to peptide sequences from the wing cuticles of migratory locusts,[64] oyster shell matrix proteins (*Pinctada* genus)[65] and chicken claw keratins.[66] Finally, His-rich SRT motifs exhibit similarity to His-rich proteins[67] of the King ragworm jaw (*Nereis virens*), another hard tissues made of sclerotized proteins that are mechanically reinforced via His-Zn coordination bonds[68-70] and dense covalent cross-linking.[71, 72]

Generally speaking, our combinatorial assay showed that Ala-rich and His-rich peptides exhibit the strongest homo-peptidic interactions and such interactions are pH-dependent, being weaker under acidic conditions and the strongest near neutral pH. Time-dependent DLS measurements demonstrate that His-rich and Ala-rich and peptides rapidly form larger complexes at neutral pH, a behavior that is particularly prominent for Ala-rich peptides (Figure 3C and D). Further examination of Ala-rich peptide aggregates by optical and SEM microscopy further indicated that these aggregates were in fact composed 30-50 nm nanofibrils bundled together into larger µm diameter fibrils (Figure 2).

The characteristic propensity of Ala-rich peptides to spontaneously self-assemble into β-sheet-rich microfibrillar structures is strongly reminiscent of amyloidogenesis, which support our previous

hypothesis that these modular repeats constitute the main source of β-sheet structure in native SRT. Their size (6 to 7 residues long) falls within the peptide length of amyloidogenic core sequences, usually four to seven amino acids.[73] In amyloid, fibril assembly is mediated by the formation of inter-peptidic β-sheet interfaces.[74] Face-to-face interactions orthogonal to the β-sheet plane occur by inter-digitation (hydrophobic interactions) or by knob-in-hole interactions involving tight packing of small residue side chains entrapped between bulkier ones.[75] Ala is one of the most abundant amino acids present in such interactions, and Ala/Val pairs have been found in many amyloid structures. With an AATAVS sequence (**A1** peptide), it is tempting to suggest that these interactions are dominant in Ala-rich SRT peptides as well. H/D exchange experiments and the quantification of solvent exchange by NMR (Figure 6) further confirm the high protection factor of all residues in this sequence (> 60% when exposed to D_2O at 65ºC for 3 days), and point to a high stability of the cross-β structure adopted by Ala-rich modular peptides, which are thus suggested to form the seeds for β-sheet supramolecular polymer network self-assembly in native SRT. Towards understanding the kinetics of assembly in SRT, a fundamental question arising is how the suckerin proteins transition from the soluble state to the supramolecular solid-state material.

CD spectroscopy studies of the peptides at different pH provide useful clues to address this question. The CD spectra indicate that our Ala-rich peptides are initially dominated by PPII conformation, with spectral features similar to those reported for other short peptides established to adopt PPII conformation.[41, 76] A consensus has emerged in the past decade that "disordered" proteins are in fact often dominated by residues that temporally adopt extended (or semi-extended) PII conformations,[39] notably for short peptides.[77, 78] For instance NMR studies demonstrated that a 7-residue poly-Ala in aqueous solution adopted a PPII conformation,[40] and similar results were obtained for the penta-peptide GGAGG.[42] Thus the PPII conformation has been suggested to be a precursor of folding for short peptides[77] as well as to represent an initial semi-extended conformation that facilitates β-sheet aggregation, which is consistent with the fact that PPII structure is closely located to the β-sheet region in the Ramachandran plot.[38, 79] Furthermore MD simulations have predicted that in the presence of water, PPII exhibits the lowest conformational free energy, whereas in the absence of water β-strand become the most stable backbone,[80] indicating that upon desolvation and/or aggregation, β-sheets can be readily nucleated from PPII conformation because their conformational energies are similar. Such a mechanism is supported here by the time-dependent CD measurements. As the pH increases and microfibers are formed from the solution, the concentration of peptide in solution decreases over time (Figure 4), with residual peptides in solution

transitioning toward β-sheets structure. Interestingly, this time-dependent evolution of CD spectra is strongly reminiscent to that reported for silk fibroins,[81] where an overall CD signature resembling those measured here for the Ala-rich peptides (Figure 4 for **A1** and **A2** peptides) has been reported, and where a strong decrease in ellipticity a few days after initial incubation has also been attributed to a decrease in protein concentration in solution. Furthermore, fibroin conformation has been shown to be strongly pH-dependent,[30] with β-sheet content increasing with pH. A reasonable potential pathway therefore emerges for suckerin peptide based fibril self-assembly, whereby small stretches of Ala-rich modules initially adopt a PPII conformation in solution, which act as a precursor for the formation of amyloid-like cross-β structures in the fibrillar state. This mechanism is also supported by our MD simulations computations. When the peptide lattice initially was allowed to relax in an unconstrained fashion, β-sheets remained strongly favored, with amplification in β-sheet content after 400 ns. Semi-quantitative FTIR of solid-state micro-fibrils as well as Congo red staining confirm that the solid-state fibrils assembled from the Ala-rich peptide solution consist of amyloid-like cross-β structures.[46]

The role of His-rich modular peptides is likely complementary to that of the Ala-rich modules. Given that charges in the full-length suckerin proteins are almost exclusively located in these modules, they are likely to play an important role for protein storage in secretory vesicles before aggregation. While the tendency of His-rich peptides to form β-sheets is weaker than Ala-rich peptides, our data indicate that the His-rich modules are nevertheless also able to form aggregates near neutral pH and above, as evidenced from DLS data (Figure 3). According to CD measurements, these peptides also tend towards β-sheet formation over time (Figure 3 for **H1** and **H2** peptides), and MD simulations also indicate that they have the capability to form cross-β structures, albeit to a lesser extent than Ala-rich modules (Figure 7C-F). Therefore, a plausible mechanism is that His-rich modular peptides play a role in maintaining the solubility of suckerins if the pH of the micro-environment where they are stored is acidic. It is increasingly recognized that the pH of secretory glands of extra-cellular materials is acidic. For instance during mussel adhesive thread formation, the pH of the glands located in the mussel feet where threads are secreted is as low as ~ 2.[34] In spider silks, the pH in spinning duct where elongation flow occurs is also acidic,[30, 31] and this tight control of pH eventually regulates the final aggregation and assembly of fibroins into silk fibers,[32, 33] with β-sheets forming from the concentrated dope under precise conditions of pH and salt concentration.[30] We suggest a similar mechanism for SRT, whereby His-rich modules contribute to maintaining a high concentration of suckerins while preventing aggregation. Upon secretion and encountering the higher pH of seawater,

the solubility of suckerin would likely decrease. Ala-rich modules that are in the semi-extended PPII conformation then have the potential to quickly form β-sheet nuclei (heterogeneous nucleation), thereby overcoming the activation energy barrier for subsequent aggregation and fibrillization (Figure 2). This phase transition into a solid polymeric network would eventually involve growth of the β-sheet nuclei extending to the His-rich domains and the collective assembly of the block co-polymeric protein into a supramolecular polymer network reinforced by β-sheet domains, as the final step of assembly. This hypothesis is supported by the very high solubility of **H1** peptide in PBS buffer (pH 7), where it remained soluble up to 50 mg/ml. A study evaluating the role of **H1** peptides in maintaining the high solubility of longer SRT peptides prior to their self-assembly into macroscopic fibers is currently on-going and will be reported in a follow-up publication.

Pro residues precisely flank Ala-rich and His-rich modules in all suckerins, and we previously postulated that this placement controls the size of β-sheets. Pro has been established as a β-sheet disruptor and exhibits the lowest propensity to form β-sheets amongst all amino acids.[82, 83] According to our DLS experiments (Figure 3), peptides containing Pro (**H2** and **A2**) form larger fibrillar structures at higher pH when compared to their counterparts without Pro, with both types of peptides found to be enriched in β-sheets by FTIR (Figure 5D-E) and Congo red (Figure 2E-F) assay. SEM observations of **A1** and **A2** microfibers reveal that the morphology of microfibers is notably different (Figure 2). While both peptides form nano-scale fibrils, those without Pro (**A1**) bundle into larger microfibers (Figure 2A-C). H/D exchange NMR studies denote strong protection factors for residues in **A2** microfibers (Figure 6B) comparable to amyloid peptides.[53, 57] However, residues in **A1** microfibers (Figure 6D) exhibit even higher protection factors. These observations suggest that the presence of Pro allows the cross β-structure packing to relax by extending the hydrogen bond lengths,[84] possibly preventing premature aggregation and in turn ensuring further assembly of the supramolecular network, which could be consistent with the higher amount of β-sheet content predicted by MD simulations for the Pro-containing **A2** peptide at equilibrium. However this assumption remains to be confirmed through further structural analysis of the peptides. In addition, Pro residues also causes a kink in the peptide backbone,[85] and this effect is likely amplified when Pro is placed in the middle of a longer peptide and not at its termini as explored here.

5. Conclusions

The present data refine our understanding for the role of modular suckerin peptides on the self-assembly of the SRT supramolecular biopolymer. A combinatorial chemistry approach identified Ala- and His-rich modular peptides as exhibiting strong inter-molecular interactions, which were then studied in detail both experimentally and by computational methods. Our results strongly suggest that Ala-rich modules of SRT act as nuclei for the initial formation of β-sheets, initially adopting PPII conformation that subsequently transform into amyloid-like cross-β structures, indicating that SRT modular peptides could be used as alternative model system to study amyloidogenesis. His-rich modules can also be involved in cross-β structures, though this ability is not as favorable. pH plays a key role, as both type of modular peptides appear to exhibit aggregation and fibrillization triggered by pH increase. Flanking Pro residues appear to play a subtle role in the stabilization of β-sheet networks. Because of their propensity to self-assemble into cross-β structures, SRT modular peptides also expand our toolkit of functional peptide-based materials for usage in various nanotechnology and health-care applications.[86]

There remain several interesting unanswered questions that will be tackled in future research. First, it has been established in the recent decade that amyloid fibrils exhibit a richer range of structures than the two-dimensional β-sheet arrangement assumed here, such as the β-solenoids, the cross-β prism, or the β-hairpin.[52] It is possible that SRT peptides form similar complex β-sheets dominated structures and we intend to conduct solid-state NMR on these peptides in the near future to answer this question. Our recent data on native SRT using SAXS has also revealed a nano-scale assembly of fibrils into a hexagonal lattice.[4] It will be of interest to reconcile this nano-scale arrangement with the peptide secondary structure. Second, Gly-rich modules were not studied in detail in this study since we focused on the modular peptides exhibiting the strongest interactions in the combinatorial assay. According to our model, Gly-rich domains are mostly amorphous[8] and play a central role in facilitating the thermo-plastic behaviour of native SRT. During thermal treatment, Gly-rich domains are suggested to exhibit viscous flow, allowing re-arrangement of the supramolecular network. Biophysical studies focusing on the Gly-rich peptides will allow a better understanding of this process. Finally, the processing pathway from a concentrated soluble form to the robust solid-state network, which could involve a pH-triggered aggregation mechanism from a concentrated colloidal phase (for instance a coacervate) or a liquid crystalline phase, is an attractive topic that also warrants further investigations.

Acknowledgments

This research was funded by the Singapore National Research Foundation (NRF) through a NRF Fellowship and a Singapore Ministry of Education (MOE) Tier 2 grant (Grant No. MOE 2011-T2-2-044) awarded to A. M.

Appendix A. Supplementary Materials

Peptide macroarray binding assay data, Congo red staining of control peptide, FTIR data, NMR spectra and simulation data referenced in text.

References

[1] J.B.M. Roger T. Hanlon, Cephalopod Behaviour, Cambridge University Press 1996.
[2] P.A. Guerette, S. Hoon, Y. Seow, M. Raida, A. Masic, F.T. Wong, V.H. Ho, K.W. Kong, M.C. Demirel, A. Pena-Francesch, S. Amini, G.Z. Tay, D. Ding, A. Miserez, Accelerating the design of biomimetic materials by integrating RNA-seq with proteomics and materials science, Nat Biotechnol 31(10) (2013) 908-915.
[3] A. Miserez, J.C. Weaver, P.B. Pedersen, T. Schneeberk, R.T. Hanlon, D. Kisailus, H. Birkedal, Microstructural and Biochemical Characterization of the Nanoporous Sucker Rings from Dosidicus gigas, Adv Mater 21(4) (2009) 401-406.
[4] V. Latza, P.A. Guerette, D. Ding, S. Amini, A. Kumar, I. Schmidt, S. Keating, N. Oxman, J.C. Weaver, P. Fratzl, A. Miserez, A. Masic, Multi-scale thermal stability of a hard thermoplastic protein-based material, Nat Commun 6 (2015) 8313.
[5] D.W. Ding, P.A. Guerette, S. Hoon, K.W. Kone, T. Cornvik, M. Nilsson, A. Kumar, J. Lescar, A. Miserez, Biomimetic Production of Silk-Like Recombinant Squid Sucker Ring Teeth Proteins, Biomacromolecules 15(9) (2014) 3278-3289.
[6] B. Cantaert, D.W. Ding, C. Rieu, L. Petrone, S. Hoon, K.H. Kock, A. Miserez, Stable Formation of Gold Nanoparticles onto Redox-Active Solid Biosubstrates Made of Squid Suckerin Proteins, Macromol Rapid Comm 36(21) (2015) 1877-1883.
[7] D.W. Ding, P.A. Guerette, J. Fu, L.H. Zhang, S.A. Irvine, A. Miserez, From Soft Self-Healing Gels to Stiff Films in Suckerin-Based Materials Through Modulation of Crosslink Density and beta-Sheet Content, Adv Mater 27(26) (2015) 3953-3961.
[8] P.A. Guerette, S. Hoon, D.W. Ding, S. Amini, A. Masic, V. Ravi, B. Venkatesh, J.C. Weaver, A. Miserez, Nanoconfined beta-Sheets Mechanically Reinforce the Supra-Biomolecular Network of Robust Squid Sucker Ring Teeth, Acs Nano 8(7) (2014) 7170-7179.
[9] S. Keten, Z.P. Xu, B. Ihle, M.J. Buehler, Nanoconfinement controls stiffness, strength and mechanical toughness of beta-sheet crystals in silk, Nat Mater 9(4) (2010) 359-367.
[10] K. Hilpert, D.F.H. Winkler, R.E.W. Hancock, Peptide arrays on cellulose support: SPOT synthesis, a time and cost efficient method for synthesis of large numbers of peptides in a parallel and addressable fashion, Nat Protoc 2(6) (2007) 1333-1349.
[11] D.v.d. Spoel, E. Lindahl, B. Hess, A.R.v. Buuren, E. Apol, P.J. Meulenhoff, D.P. Tieleman, A.L.T.M. Sijbers, K.A. Feenstra, R.v. Drunen, H.J.C. Berendsen, Gromacs User Manual version 4.5, www.gromacs.org. 2010).
[12] H. Bekker, H.J.C. Berendsen, E.J. Dijkstra, S. Achterop, R. Vondrumen, D. Vanderspoel, A. Sijbers, H. Keegstra, B. Reitsma, M.K.R. Renardus, Gromacs - a Parallel Computer for Molecular-Dynamics Simulations, Physics Computing '92, World Scientific Publishing, 1993, pp. 252-256.
[13] H.J.C. Berendsen, D. Vanderspoel, R. Vandrunen, Gromacs - a Message-Passing Parallel Molecular-Dynamics Implementation, Comput Phys Commun 91(1-3) (1995) 43-56.

[14] E. Lindahl, B. Hess, D. van der Spoel, GROMACS 3.0: a package for molecular simulation and trajectory analysis, J Mol Model 7(8) (2001) 306-317.
[15] D. Van der Spoel, E. Lindahl, B. Hess, G. Groenhof, A.E. Mark, H.J.C. Berendsen, GROMACS: Fast, flexible, and free, J Comput Chem 26(16) (2005) 1701-1718.
[16] B. Hess, C. Kutzner, D. van der Spoel, E. Lindahl, GROMACS 4: Algorithms for highly efficient, load-balanced, and scalable molecular simulation, J Chem Theory Comput 4(3) (2008) 435-447.
[17] G. Bussi, D. Donadio, M. Parrinello, Canonical sampling through velocity rescaling, J Chem Phys 126(1) (2007) 014101.
[18] S. Nose, M.L. Klein, Constant Pressure Molecular-Dynamics for Molecular-Systems, Mol Phys 50(5) (1983) 1055-1076.
[19] T. Darden, D. York, L. Pedersen, Particle Mesh Ewald - an N.Log(N) Method for Ewald Sums in Large Systems, J Chem Phys 98(12) (1993) 10089-10092.
[20] W.L. Jorgensen, J. Chandrasekhar, J.D. Madura, R.W. Impey, M.L. Klein, Comparison of Simple Potential Functions for Simulating Liquid Water, J Chem Phys 79(2) (1983) 926-935.
[21] A.D. MacKerell, D. Bashford, M. Bellott, R.L. Dunbrack, J.D. Evanseck, M.J. Field, S. Fischer, J. Gao, H. Guo, S. Ha, D. Joseph-McCarthy, L. Kuchnir, K. Kuczera, F.T.K. Lau, C. Mattos, S. Michnick, T. Ngo, D.T. Nguyen, B. Prodhom, W.E. Reiher, B. Roux, M. Schlenkrich, J.C. Smith, R. Stote, J. Straub, M. Watanabe, J. Wiorkiewicz-Kuczera, D. Yin, M. Karplus, All-atom empirical potential for molecular modeling and dynamics studies of proteins, J Phys Chem B 102(18) (1998) 3586-3616.
[22] A.D. Mackerell, M. Feig, C.L. Brooks, Extending the treatment of backbone energetics in protein force fields: Limitations of gas-phase quantum mechanics in reproducing protein conformational distributions in molecular dynamics simulations, J Comput Chem 25(11) (2004) 1400-1415.
[23] A.T. Nguyen, Q.L. Huang, Z. Yang, N.B. Lin, G.Q. Xu, X.Y. Liu, Crystal Networks in Silk Fibrous Materials: From Hierarchical Structure to Ultra Performance, Small 11(9-10) (2015) 1039-1054.
[24] E. Monsellier, F. Chiti, Prevention of amyloid-like aggregation as a driving force of protein evolution, Embo Rep 8(8) (2007) 737-742.
[25] S. Rauscher, S. Baud, M. Miao, F.W. Keeley, R. Pomes, Proline and glycine control protein self-organization into elastomeric or amyloid fibrils, Structure 14(11) (2006) 1667-1676.
[26] H. Benyamini, A. Friedler, Using peptides to study protein-protein interactions, Future Med Chem 2(6) (2010) 989-1003.
[27] C. Katz, L. Levy-Beladev, S. Rotem-Bamberger, T. Rito, S.G.D. Rudiger, A. Friedler, Studying protein-protein interactions using peptide arrays, Chem Soc Rev 40(5) (2011) 2131-2145.
[28] K.S. Lam, M. Lebl, V. Krchnak, The ''one-bead-one-compound'' combinatorial library method, Chem Rev 97(2) (1997) 411-448.
[29] K.S. Lam, S.E. Salmon, E.M. Hersh, V.J. Hruby, W.M. Kazmierski, R.J. Knapp, A New Type of Synthetic Peptide Library for Identifying Ligand-Binding Activity, Nature 354(6348) (1991) 82-84.
[30] C. Dicko, F. Vollrath, J.M. Kenney, Spider silk protein refolding is controlled by changing pH, Biomacromolecules 5(3) (2004) 704-710.
[31] F. Vollrath, D.P. Knight, Liquid crystalline spinning of spider silk, Nature 410(6828) (2001) 541-548.
[32] G. Askarieh, M. Hedhammar, K. Nordling, A. Saenz, C. Casals, A. Rising, J. Johansson, S.D. Knight, Self-assembly of spider silk proteins is controlled by a pH-sensitive relay, Nature 465(7295) (2010) 236-239.
[33] F. Hagn, C. Thamm, T. Scheibel, H. Kessler, pH-Dependent Dimerization and Salt-Dependent Stabilization of the N-terminal Domain of Spider Dragline Silk-Implications for Fiber Formation, Angew Chem Int Edit 50(1) (2011) 310-313.
[34] L. Petrone, A. Kumar, C.N. Sutanto, N.J. Patil, S. Kannan, A. Palaniappan, S. Amini, B. Zappone, C. Verma, A. Miserez, Mussel adhesion is dictated by time-regulated secretion and molecular conformation of mussel adhesive proteins, Nat Commun 6 (2015) 8737.
[35] A.H. Simmons, C.A. Michal, L.W. Jelinski, Molecular orientation and two-component nature of the crystalline fraction of spider dragline silk, Science 271(5245) (1996) 84-87.
[36] N.J. Greenfield, Using circular dichroism spectra to estimate protein secondary structure, Nat Protoc 1(6) (2006) 2876-2890.

[37] N. Sreerama, R.W. Woody, Structural composition of beta(I)- and beta(II)-proteins, Protein Sci 12(2) (2003) 384-388.
[38] A.A. Adzhubei, M.J. Sternberg, A.A. Makarov, Polyproline-II helix in proteins: structure and function, J Mol Biol 425(12) (2013) 2100-2132.
[39] J.L.S. Lopes, A.J. Miles, L. Whitmore, B.A. Wallace, Distinct circular dichroism spectroscopic signatures of polyproline II and unordered secondary structures: Applications in secondary structure analyses, Protein Sci 23(12) (2014) 1765-1772.
[40] Z.S. Shi, C.A. Olson, G.D. Rose, R.L. Baldwin, N.R. Kallenbach, Polyproline II structure in a sequence of seven alanine residues, P Natl Acad Sci USA 99(14) (2002) 9190-9195.
[41] Z.S. Shi, K. Chen, Z.G. Liu, A. Ng, W.C. Bracken, N.R. Kallenbach, Polyproline II propensities from GGXGG peptides reveal an anticorrelation with beta-sheet scales, P Natl Acad Sci USA 102(50) (2005) 17964-17968.
[42] L. Ding, K. Chen, P.A. Santini, Z.S. Shi, N.R. Kallenbach, The pentapeptide GGAGG has PII conformation, J Am Chem Soc 125(27) (2003) 8092-8093.
[43] J. Kong, S. Yu, Fourier transform infrared spectroscopic analysis of protein secondary structures, Acta Bioch Bioph Sin 39(8) (2007) 549-559.
[44] A. Barth, C. Zscherp, What vibrations tell us about proteins, Q Rev Biophys 35(4) (2002) 369-430.
[45] S. Mukherjee, P. Chowdhury, F. Gai, Effect of Dehydration on the Aggregation Kinetics of Two Amyloid Peptides, J Phys Chem B 113(2) (2009) 531-535.
[46] R. Nelson, D. Eisenberg, Structural models of amyloid-like fibrils, Adv Protein Chem 73 (2006) 235-282.
[47] C.L. Masters, K. Beyreuther, M. Trillet, Amyloid Protein Precursor in Development, Aging and Alzheimer's Disease, Springer-Verlag Berlin Heidelberg2013.
[48] R. Khurana, V.N. Uversky, L. Nielsen, A.L. Fink, Is Congo red an amyloid-specific dye?, J Biol Chem 276(25) (2001) 22715-22721.
[49] R. Nelson, M.R. Sawaya, M. Balbirnie, A.O. Madsen, C. Riekel, R. Grothe, D. Eisenberg, Structure of the cross-beta spine of amyloid-like fibrils, Nature 435(7043) (2005) 773-778.
[50] M.R. Sawaya, S. Sambashivan, R. Nelson, M.I. Ivanova, S.A. Sievers, M.I. Apostol, M.J. Thompson, M. Balbirnie, J.J.W. Wiltzius, H.T. McFarlane, A.O. Madsen, C. Riekel, D. Eisenberg, Atomic structures of amyloid cross-beta spines reveal varied steric zippers, Nature 447(7143) (2007) 453-457.
[51] L.K. Chang, J.H. Zhao, H.L. Liu, K.T. Liu, J.T. Chen, W.B. Tsai, Y. Ho, Molecular Dynamics Simulations to Investigate the Structural Stability and Aggregation Behavior of the GGVVIA Oligomers Derived from Amyloid beta Peptide, J Biomol Struct Dyn 26(6) (2009) 731-740.
[52] A.V. Kajava, J.M. Squire, D.A. Parry, Beta-structures in fibrous proteins, Adv Protein Chem 73 (2006) 1-15.
[53] J.H. Ippel, A. Olofsson, J. Schleucher, E. Lundgren, S.S. Wijmenga, Probing solvent accessibility of amyloid fibrils by solution NMR spectroscopy, P Natl Acad Sci USA 99(13) (2002) 8648-8653.
[54] Y.Z. Zhang, Y. Paterson, H. Roder, Rapid Amide Proton-Exchange Rates in Peptides and Proteins Measured by Solvent Quenching and 2-Dimensional Nmr, Protein Sci 4(4) (1995) 804-814.
[55] N. Hirota-Nakaoka, K. Hasegawa, H. Naiki, Y. Goto, Dissolution of beta(2)-microglobulin amyloid fibrils by dimethylsulfoxide, J Biochem 134(1) (2003) 159-164.
[56] K. Wüthrich, NMR of Proteins and Nucleic Acids, Wiley, New York1986.
[57] A. Olofsson, A.E. Sauer-Eriksson, A. Ohman, The solvent protection of Alzheimer amyloid-beta-(1-42) fibrils as determined by solution NMR spectroscopy, J Biol Chem 281(1) (2006) 477-483.
[58] F.G. Quiroz, A. Chilkoti, Sequence heuristics to encode phase behaviour in intrinsically disordered protein polymers, Nat Mater 14(11) (2015) 1164-1172.
[59] J. Danielsson, J. Jarvet, P. Damberg, A. Graslund, The Alzheimer beta-peptide shows temperature-dependent transitions between left-handed 3(1)-helix, beta-strand and random coil secondary structures, Febs J 272(15) (2005) 3938-3949.
[60] J.M. Gosline, P.A. Guerette, C.S. Ortlepp, K.N. Savage, The mechanical design of spider silks: From fibroin sequence to mechanical function, J Exp Biol 202(23) (1999) 3295-3303.
[61] R.V. Lewis, Spider silk: Ancient ideas for new biomaterials, Chem Rev 106(9) (2006) 3762-3774.
[62] C.Y. Hayashi, R.V. Lewis, Molecular architecture and evolution of a modular spider silk protein gene, Science 287(5457) (2000) 1477-1479.

[63] J. Gatesy, C. Hayashi, D. Motriuk, J. Woods, R. Lewis, Extreme diversity, conservation, and convergence of spider silk fibroin sequences, Science 291(5513) (2001) 2603-2605.
[64] T.N. Krogh, L. Skou, P. Roepstorff, S.O. Andersen, P. Hojrup, Primary Structure of Proteins from the Wing Cuticle of the Migratory Locust, Locusta-Migratoria, Insect Biochem Molec 25(3) (1995) 319-329.
[65] S. Sudo, T. Fujikawa, T. Nagakura, T. Ohkubo, K. Sakaguchi, M. Tanaka, K. Nakashima, T. Takahashi, Structures of mollusc shell framework proteins, Nature 387(6633) (1997) 563-564.
[66] L.A. Whitbread, K. Gregg, G.E. Rogers, The Structure and Expression of a Gene Encoding Chick Claw Keratin, Gene 101(2) (1991) 223-229.
[67] C.C. Broomell, S.F. Chase, T. Laue, J.H. Waite, Cutting edge structural protein from the jaws of Nereis virens, Biomacromolecules 9(6) (2008) 1669-1677.
[68] C.C. Broomell, M.A. Mattoni, F.W. Zok, J.H. Waite, Critical role of zinc in hardening of Nereis jaws, J Exp Biol 209(16) (2006) 3219-3225.
[69] C.C. Broomell, F.W. Zok, J.H. Waite, Role of transition metals in sclerotization of biological tissue, Acta Biomater 4(6) (2008) 2045-2051.
[70] H.C. Lichtenegger, T. Schoberl, J.T. Ruokolainen, J.O. Cross, S.M. Heald, H. Birkedal, J.H. Waite, G.D. Stucky, Zinc and mechanical prowess in the jaws of Nereis, a marine worm, P Natl Acad Sci USA 100(16) (2003) 9144-9149.
[71] H. Birkedal, R.K. Khan, N. Slack, C. Broomell, H.C. Lichtenegger, F. Zok, G.D. Stucky, J.H. Waite, Halogenated veneers: Protein cross-linking and halogenation in the jaws of Nereis, a marine polychaete worm, Chembiochem 7(9) (2006) 1392-1399.
[72] R.K. Khan, P.K. Stoimenov, T.E. Mates, J.H. Waite, G.D. Stucky, Exploring gradients of halogens and zinc in the surface and subsurface of Nereis jaws, Langmuir 22(20) (2006) 8465-8471.
[73] J.D. Pham, N. Chim, C.W. Goulding, J.S. Nowick, Structures of Oligomers of a Peptide from beta-Amyloid (vol 135, pg 12460, 2013), J Am Chem Soc 136(11) (2014) 4446-4446.
[74] J.D. Pham, R.K. Spencer, K.H. Chen, J.S. Nowick, A Fibril-Like Assembly of Oligomers of a Peptide Derived from beta-Amyloid, J Am Chem Soc 136(36) (2014) 12682-12690.
[75] P.N. Cheng, J.D. Pham, J.S. Nowick, The Supramolecular Chemistry of beta-Sheets, J Am Chem Soc 135(15) (2013) 5477-5492.
[76] Z.G. Liu, K. Chen, A. Ng, Z.S. Shi, R.W. Woody, N.R. Kallenbach, Solvent dependence of PII conformation in model alanine peptides, J Am Chem Soc 126(46) (2004) 15141-15150.
[77] T.P. Creamer, M.N. Campbell, Determinants of the polyproline II helix from modeling studies, 2002.
[78] Z.S. Shi, K. Chen, Z.G. Liu, N.R. Kallenbach, Conformation of the backbone in unfolded proteins, Chem Rev 106(5) (2006) 1877-1897.
[79] B. Bochicchio, A.M. Tamburro, Polyproline II structure in proteins: Identification by chiroptical spectroscopies, stability, and functions, Chirality 14(10) (2002) 782-792.
[80] R.L. Baldwin, A new perspective on unfolded proteins, Unfolded Proteins 62 (2002) 361-367.
[81] C. Dicko, D. Knight, J.M. Kenney, F. Vollrath, Structural conformation of spidroin in solution: a synchrotron radiation circular dichroism study, Biomacromolecules 5(3) (2004) 758-767.
[82] D.L. Minor, P.S. Kim, Measurement of the Beta-Sheet-Forming Propensities of Amino-Acids, Nature 367(6464) (1994) 660-663.
[83] C.K. Smith, J.M. Withka, L. Regan, A Thermodynamic Scale for the Beta-Sheet Forming Tendencies of the Amino-Acids, Biochemistry-Us 33(18) (1994) 5510-5517.
[84] S.Y. Sheu, D.Y. Yang, H.L. Selzle, E.W. Schlag, Energetics of hydrogen bonds in peptides, P Natl Acad Sci USA 100(22) (2003) 12683-12687.
[85] C.M. Deber, A.G. Therien, Putting the beta-breaks on membrane protein misfolding, Nat Struct Biol 9(5) (2002) 318-319.
[86] C. Aleman, A. Bianco, M. Venanzi, Peptide Materials: From Nanostructures to Applications, Wiley2013.

Figure Legends

Figure 1. Suckerin peptide macroarray binding assay. (A) Full-length amino acid sequence of suckerin-19, with alignment highlighting the main modular peptides (bold: signal peptide; red shaded: Ala-rich and His-rich module; blue shaded: Gly-rich modules). **(B**) Peptide macroarray binding experiment: ligand peptides were immobilized onto a cellulose membrane and acetylated to cap the free amine. The fluorescent-tagged peptide analytes were then incubated, followed by stringent washing. See Methods section for details. **(C)** Heatmap of the binding assay with relative interaction strength obtained from the fluorescence intensity of each spot (blue shading: low level of interactions; red shading: high level of interactions). Average intensity values were obtained from quadruplicate screeing of each interaction. The boxed diagonals indicate the intensity values derived from homo-interactions of a single peptide.

Figure 2. Congo red staining and SEM micrographs of microfibers self-assembled from peptides A1 and A2. Microfibers formed from peptide A1 at pH 4 **(A)**, pH 7 **(B)**, and pH 8.6 **(C)**. Microfibers formed by peptide A2 at pH 4 **(D)**, pH 7 **(E)**, and pH 8.6 **(F)**. Self-assembled microfibers stained with Congo red dye were viewed under bright field (upper left corners) and polarized light microscopy (lower left corners). All microfibers display apple-green birefringent properties when viewed under polarized light, indicating the presence of amyloid-like cross-β structures.

Figure 3. Self-assembly of peptides monitored by dynamic light scattering. Peptides were incubated at pH 4 (red), 7 (green) and 8.6 (blue) at 50 μM peptide concentration. The peptides were also incubated in hydrogen-bond disrupting urea (black), serving as monomeric state controls (equilibrium state with the minimum self-assembly). **(A)** Peptide H1; **(B)** H2; **(C)** A1 and **(D)** A2.

Figure 4. Circular dichroism spectra of peptides monitored over 50 day time period. All four peptides were incubated in buffers at pH 4, 7 and 8.6 over a period of 50 days and spectra were collected at different times. **Column 1,** Peptide H1; **column 2,** H2; **column 3,** A1; **column 4,** A2. Insets at pH 7 are zoom-in of the low ellipticity intensity spectra after 28 days (Ala-rich peptides) and 14 days (His-rich peptides).

Figure 5. ATR-FTIR spectra of Ala-rich peptides self-assembled into microfibers. Spectra were obtained for peptide microfibers formed at pH 4, 7 and 8.6. Insets show the zoomed-in regions of the Amide I band that was used for deconvolution of the original spectra, with sub-band location determined by maxima of inverted secondary derivative of the spectra. Peptide A1 at pH 4 **(A)**; pH 7 **(B)**; and pH 8.6 **(C).** Peptide A2 at pH 4 **(D)**; pH 7 **(E)**, and pH 8.6 **(F).**

Figure 6. 1D ^{1}H NMR H/D exchange studies on peptides A1 and A2. (A) 1D ^{1}H NMR spectra of peptide A1 microfibers showing the decrease in signal intensities as temperature increases; **(B)** Peptide A1 residue specific

hydrogen-exchange profiles as a function of temperature; **(C)** 1D ^{1}H NMR spectra of peptide A2 microfibers; **(D)** peptide A2 residue specific hydrogen-exchange profile as a function of temperature.

Figure 7. Molecular dynamics simulations of suckerin peptide fibers. Peptides were arranged in an anti-parallel fashion to impose a fibril setting that simulates the self-assembled β-sheet network of SRT peptides. **(A)** Hydrogen bond count and **(B)** β-sheet count from each peptide's MD simulation recorded at 0 and 200 ns of simulation. **(C)** The snapshot of simulated structure of peptide H1 at 200 ns at pH 4 (left) and pH7 (right), which did not show a stable β-sheet network of fibrils. **(D)** The snapshot of simulated structure of peptide H2 at 200 ns, illustrating partial stacking of peptides that was maintained at both pH4 (left) and pH7 (right). Final simulated structure of **(E)** peptide A1 and **(F)** peptide A2, showing highly stable fibrillar stacking structures (no differences between pH 4 and pH 7 were observed) with an increase in hydrogen bond and β-sheet counts for peptide A2 over time.

Tables

Table 1. Modular peptides from Suckerin-19 protein selected for this study, together with protein-based peptides exhibiting sequence homology with the suckerin peptides.

	Sequence	Code	Peptide Similarity
1	Ac-**GGY**-$CONH_2$	G1	Spider silk, Migratory locust wing cuticle, Oyster shell matrix, Chicken claw keratin
2	Ac-**GGLY**-$CONH_2$	G2	
3	Ac-**GLGGY**-$CONH_2$	G3	
4	Ac-**HTTHHA**-$CONH_2$	H1	Humboldt Squid beak, King ragworm jaw
5	Ac-**HTTHHAP**-$CONH_2$	H2	
6	Ac-**AATAVS**-$CONH_2$	A1	Spider silk, Migratory locust wing cuticle, Oyster shell matrix, Chicken claw keratin
7	Ac-**PAATAVS**-$CONH_2$	A2	

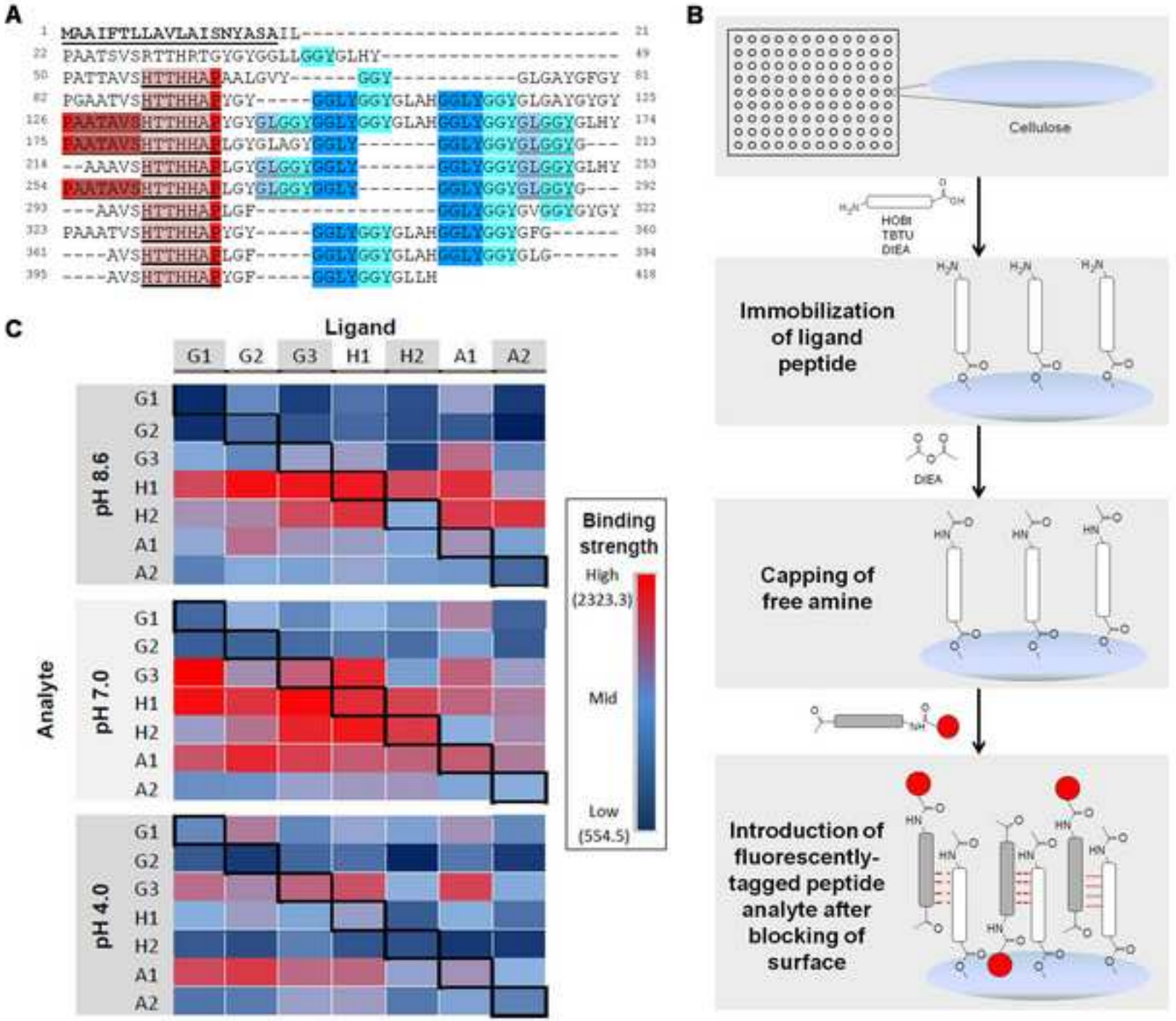

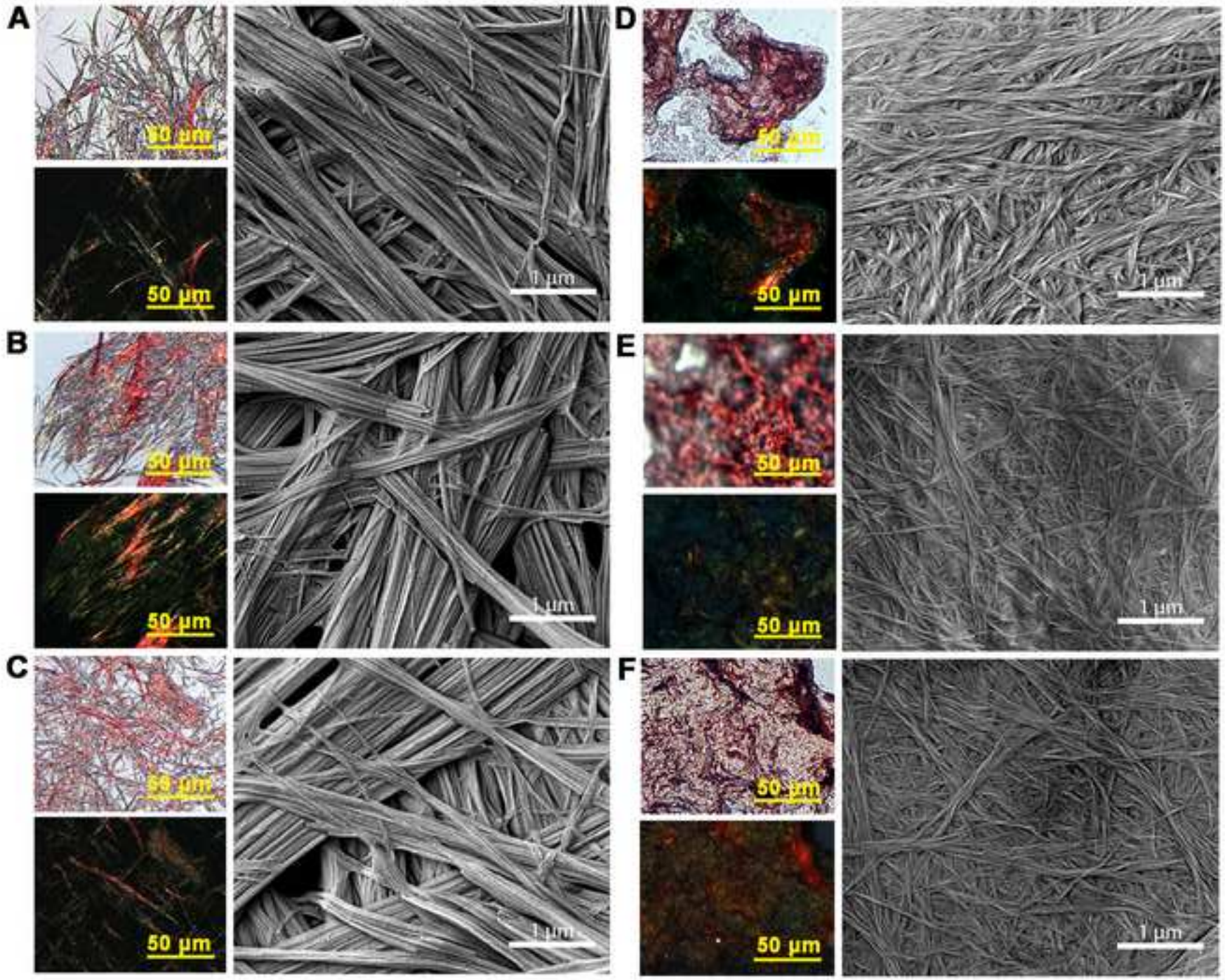

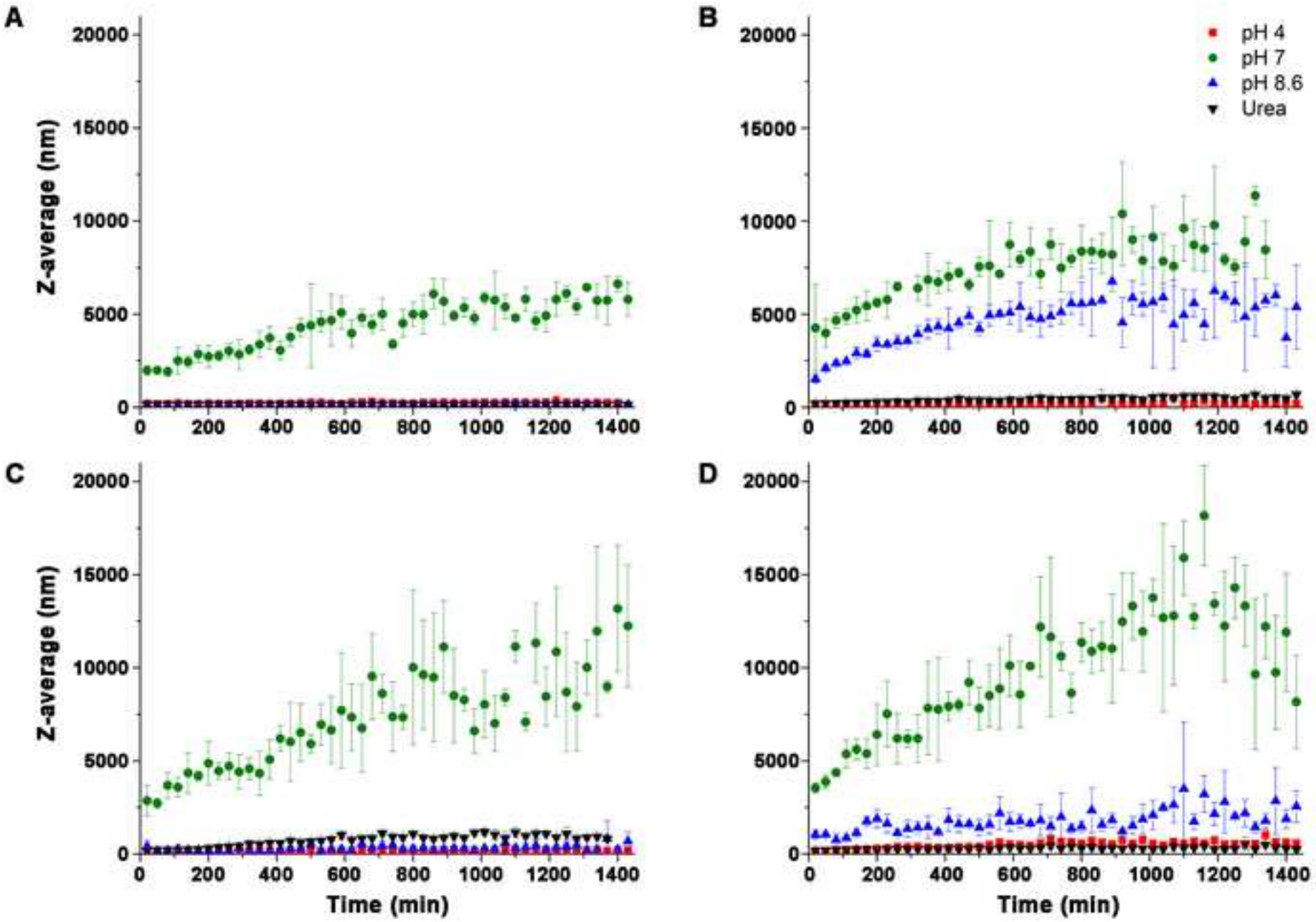

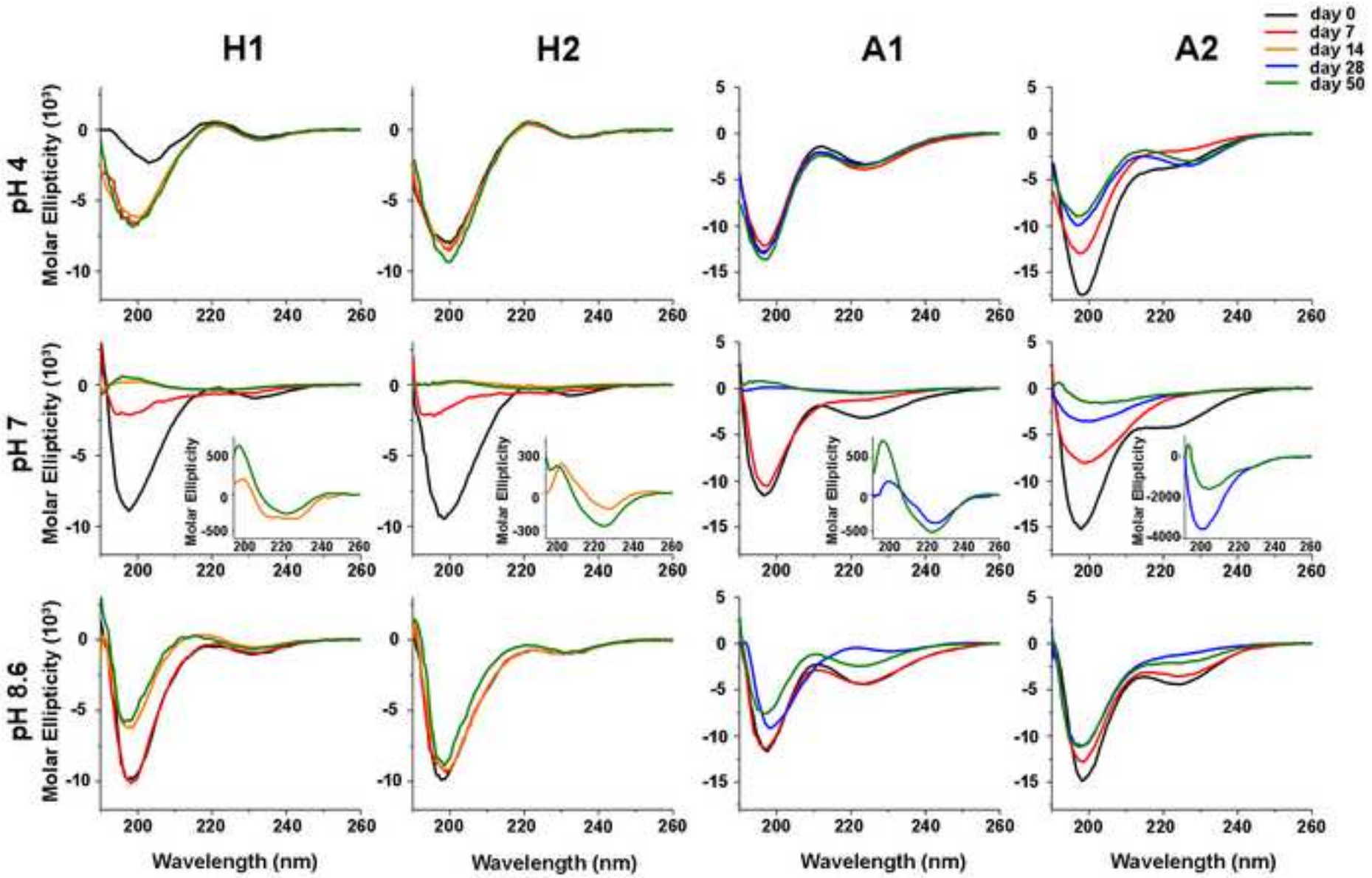

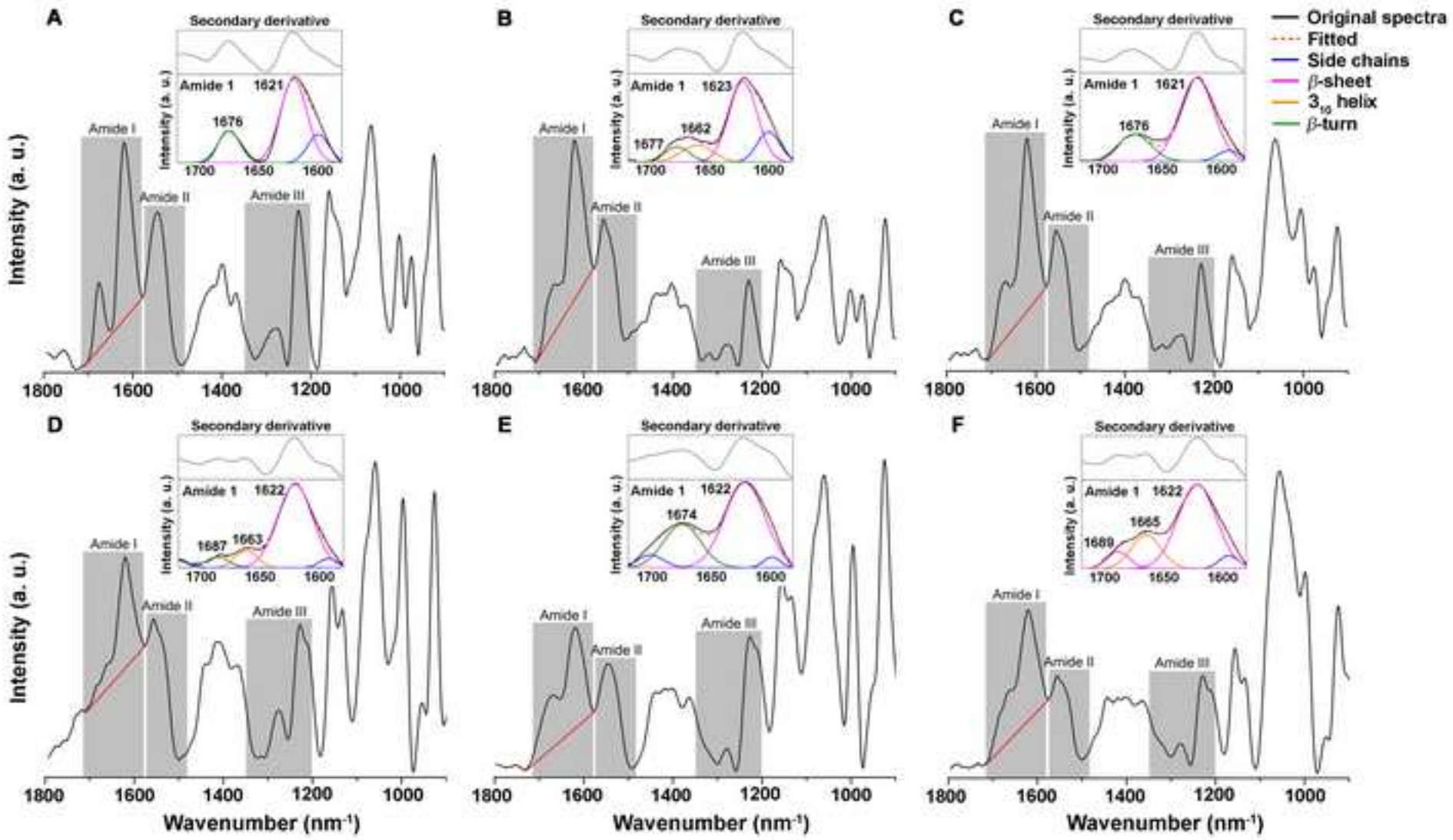

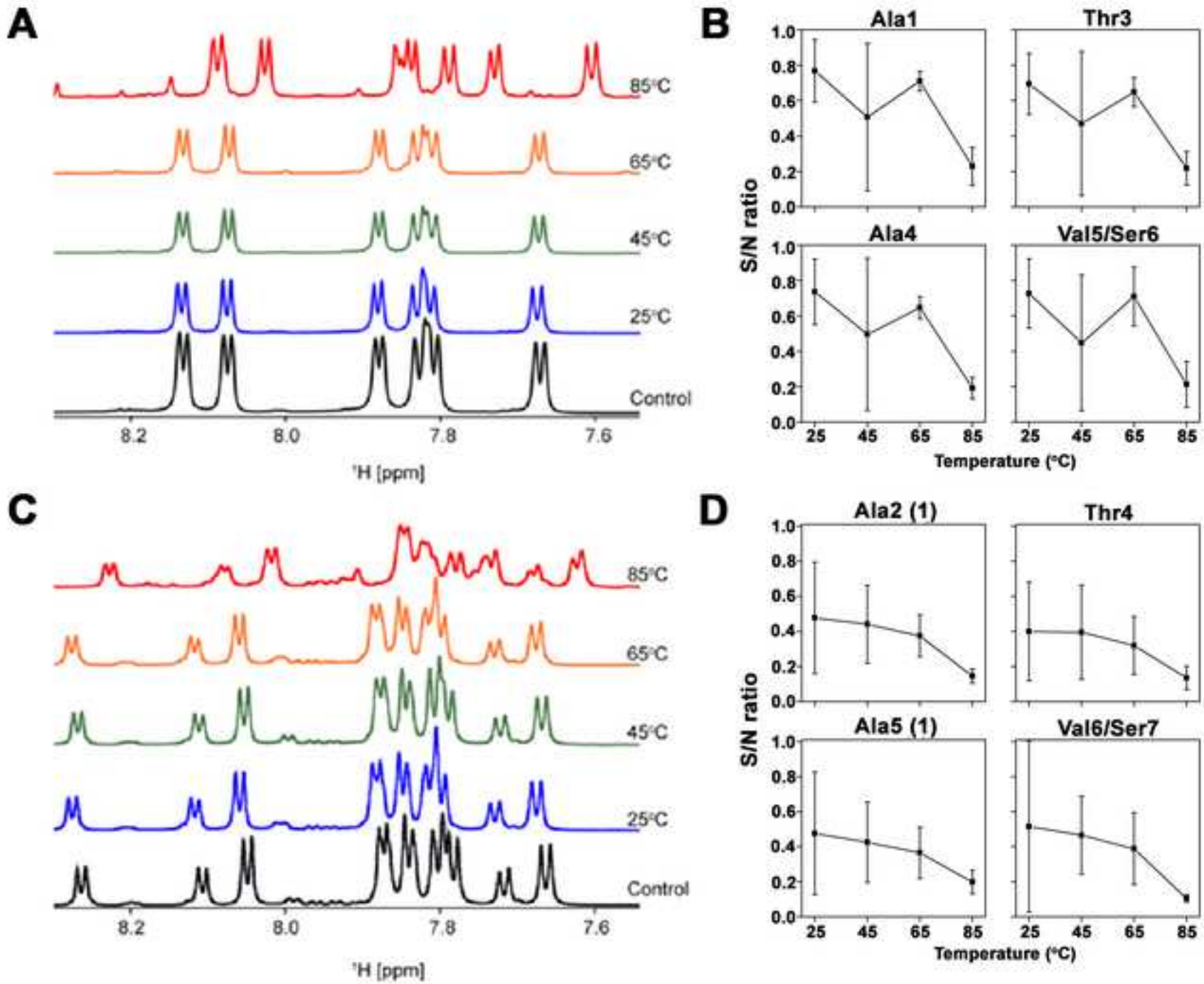

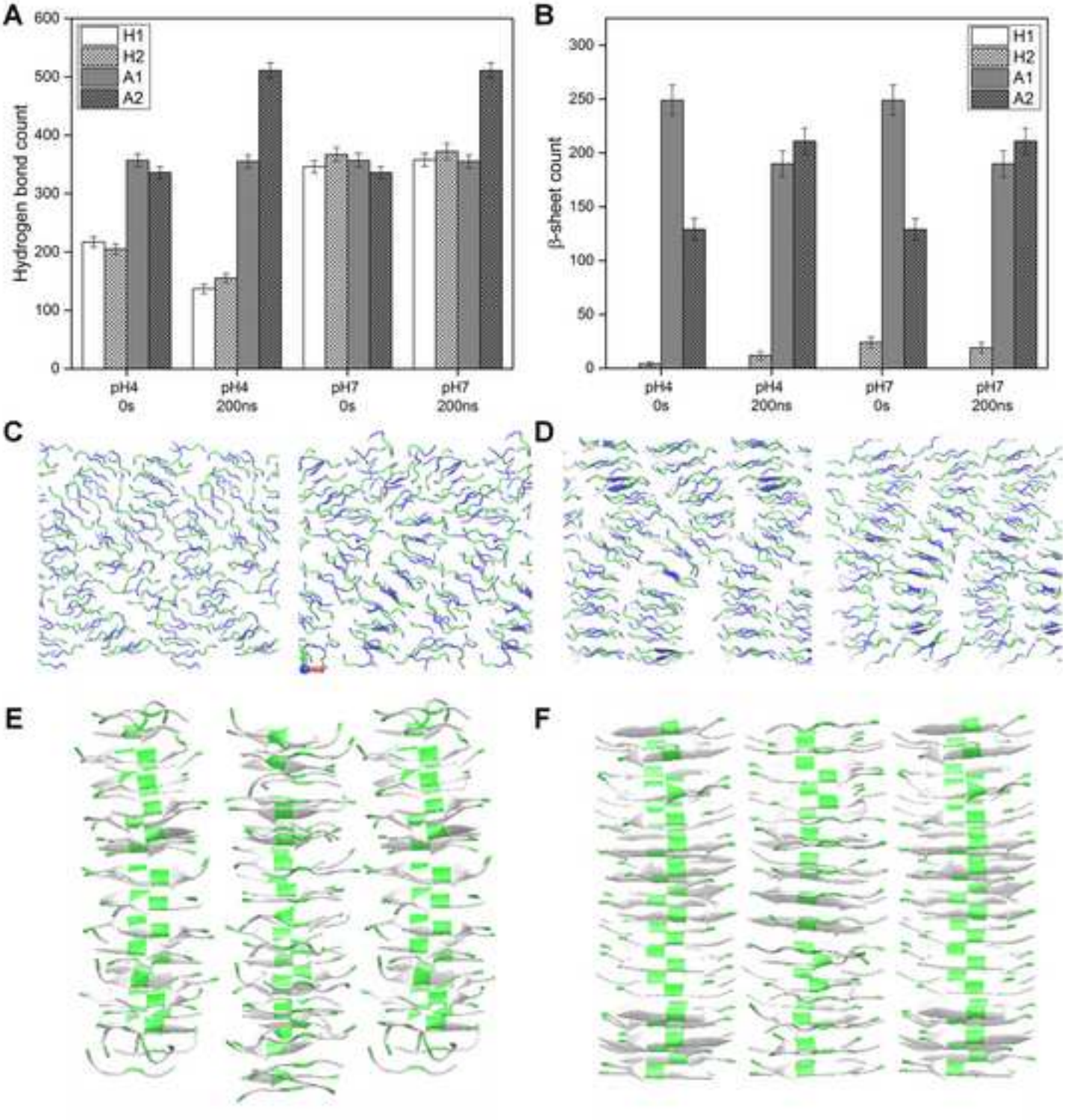

Ala rich
His rich
Gly rich (GGY/GGLY/GLGGY)

Modular sequence of Suckerin-19

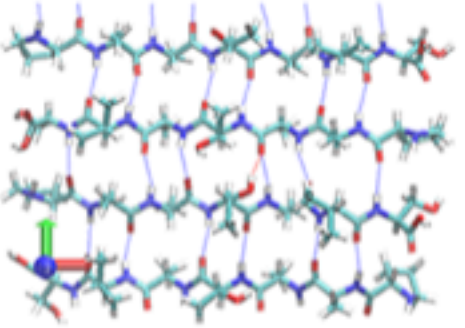

β-sheet building blocks

Humboldt Squid Sucker Ring Teeth

Mapping binding interactions of Suckerin peptides

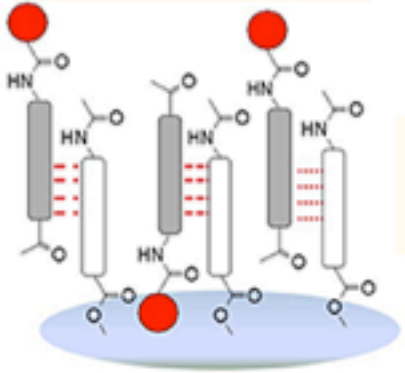

Self-assembly of Suckerin peptides

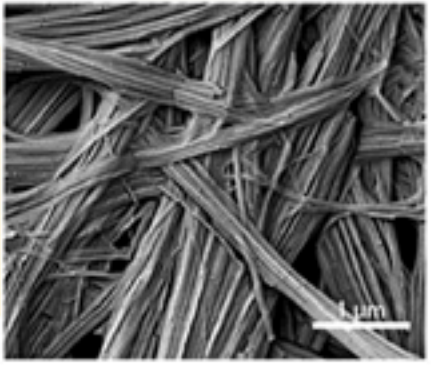

In recent years, the sucker ring teeth (SRT) located on the arms and tentacles of cephalopods have emerged as a very promising protein-based biopolymer with the potential to rival silk in biomedical and engineering applications. SRT are made of modular, block co-polymer like proteins (suckerins), which assemble into a semi-crystalline polymer reinforced by nano-confined β-sheets, resulting in a supramolecular network with mechanical properties that match those of the strongest engineering polymers. In this study, we aimed to understand the molecular mechanisms behind SRT's self-assembly and robustness. The most abundant modular peptidic blocks of suckerin proteins were studied by various spectroscopic methods. Using CD, FTIR and Congo red staining methods, we demonstrate that SRT peptides form amyloid-like cross-β structures.